Ore Geology Reviews 73 (2016) 330–345

Contents lists available at ScienceDirect

Ore Geology Reviews

journal homepage: www.elsevier.com/locate/oregeorev

Redox states and genesis of magmas associated with intra-continental porphyry Cu–Au mineralization within the Jinshajiang–Red River alkaline igneous belt, SW China

Leiluo Xu [a], Xianwu Bi [a], Ruizhong Hu [a,*], Youqiang Qi [a], Yongyong Tang [a], Xinsong Wang [a,b], Jingjing Zhu [a]

[a] State Key Laboratory of Ore Deposit Geochemistry, Institute of Geochemistry, Chinese Academy of Sciences, Guiyang 550002, China
[b] Graduate University of Chinese Academy of Sciences, Beijing 100049, China

ARTICLE INFO

Article history:
Received 30 April 2014
Received in revised form 5 May 2015
Accepted 6 May 2015
Available online 8 May 2015

Keywords:
Redox states
Genesis
Ce^{4+}/Ce^{3+} ratios of zircon
Cu–Au ore-bearing and barren porphyry intrusions
Jinshajiang–Red River alkaline igneous belt

ABSTRACT

The Jinshajiang–Red River alkaline igneous belt and the associated Cenozoic Cu–Au mineralization are located in an intra-continental strike-slip fault zone in SW China. The Ce^{4+}/Ce^{3+} ratios of zircon from representative Cu-mineralized, Au-mineralized and barren porphyry intrusions from the belt indicate that the Cu–Au ore-bearing porphyry intrusions had much higher fO_2 of magma than the barren porphyry intrusions. Elemental and Sr–Nd isotope ratio data indicate that both the Cu–Au ore-bearing and barren porphyry intrusions were derived from partial melts of the ancient enriched metasomatized mantle sources (EMII type). The mantle source was possibly modified by subduction of the Paleo-Tethyan oceanic slab beneath the Changdu–Simao block between the early Permian and the late Triassic. The oxygen fugacity of the magma was likely related to the redox state of the source, and the different fO_2 calculated for the magmas that gave rise to Cu–Au ore-bearing and barren porphyry intrusions are a product of magmas from the different sources. The sources of the barren porphyry intrusions were influenced mainly by the slab-derived fluids, whereas the sources of the Cu–Au ore-bearing porphyry intrusions were modified by both the slab-derived fluids and slab-derived melts. Cenozoic strike-slip faulting in this region caused lithospheric-scale extension and upwelling of the asthenosphere; the heat produced by this process produced partial melts of the ancient enriched metasomatized mantle sources, resulting in the emplacement of alkaline porphyry intrusions and associated Cu–Au mineralization at ~40–30 Ma.

1. Introduction

Porphyry Cu–Au systems are usually associated with calc-alkaline and alkaline igneous rocks, and they are primarily formed in arc environments (Sillitoe, 1972, 1997, 2002, 2010; Mitchell, 1973; Tatsumi, 1989; Richards, 1990, 2003; Muller and Groves, 1993; Ulrich et al., 1999; Ulrich and Heinrich, 2001; Hattori and Keith, 2001; Muller, 2002; Mungall, 2002; Heinrich et al., 2005). Porphyry Cu–Au mineralization in arc-settings is thought to be closely related to relatively oxidized calc-alkaline and alkaline magmas (Sillitoe, 1972, 1997, 2002, 2010; Richards, 1990, 2003, 2009, 2011a; Muller and Groves, 1993; Ulrich et al., 1999; Ulrich and Heinrich, 2001; Oyarzun et al., 2001; Mungall, 2002; Ballard et al., 2002; Imai et al., 1993; Imai, 2002, 2004; Sun et al., 2004, 2013). This association can be ascribed to the redox control of oxygen fugacity (fO_2) on the speciation and solubility of sulfur in a magma, and the influence of fO_2 on the fractionation of Cu- and Au-sulfides from a magma (Ballard et al., 2002; Mungall, 2002); under high fO_2 conditions, the majority of the sulfur exists as SO_2 or SO_4^{2-} with very low concentrations of S^{2-} in a magma; this prevents saturation and precipitation of immiscible Cu- and Au-sulfides from a fractionating magma, thus, allowing concentration of Cu and Au during magmatic differentiation and eventually their localization in magmatic–hydrothermal ore-forming fluids (Carroll and Rutherford, 1987; Spooner, 1993; Wybon, 1994; Sillitoe, 1997; Streck and Dilles, 1998; Mungall, 2002; Richards, 2003; Sun et al., 2004, 2013). Numerous studies have suggested that the high fO_2 of arc-magmas which gave rise to porphyry Cu–Au mineralization, were primarily produced by oxidized silicate melts or hydrothermal fluids, released from a subducted oceanic slab (Wyllie, 1978; Tatsumi, 1989; Davies and Stevenson, 1992; Peacock, 1993; McInnes and Cameron, 1994; Brandon and Draper, 1996; Mungall, 2002; Oyarzun et al., 2008). There are also abundant porphyry Cu–Au systems in intra-continental settings (Hu et al., 1998, 2004; Bi et al., 2002, 2004, 2005, 2006, 2009; Hou et al., 2003a,b, 2004, 2007, 2011, 2013; Richards, 2009; Liu et al., 2012; Lu et al., 2013; Zhang et al., 2013); examples include the Cenozoic porphyry Cu–Au systems in the Jinshajiang–Red River alkaline igneous belt, SW China, the Mesozoic Dexing porphyry Cu(Mo–Au) system in eastern China, and the Miocene Gangdese porphyry Cu(Mo) belt in Tibet, western China (Hu et al., 1998, 2004; Bi et al., 2002, 2004, 2005, 2009; Hou et al., 2003a,b, 2004, 2007, 2011, 2013; Xu et al., 2010; Liu et al., 2012; Lu et al., 2013). These porphyry Cu–Au systems are usually linked to

* Corresponding author.
E-mail address: huruizhong@vip.gyig.ac.cn (R. Hu).

http://dx.doi.org/10.1016/j.oregeorev.2015.05.007
0169-1368/

intermediate-acidic rocks that belong to a group of high-K calc-alkaline and shoshonitic magma series, and are not considered to be directly related to subduction of the oceanic slabs (Hou et al., 2004, 2007, 2011, 2013; Liu et al., 2012). In comparison with porphyry Cu–Au systems in arc-settings, the fO_2 of magmas associated with porphyry Cu–Au mineralization in intra-continental settings is not well understood. A few studies indicate that the magmas associated with intra-continental porphyry Cu–Au mineralization had elevated fO_2 (Liang et al., 2006a,b; Bi et al., 2006, 2009; Zhang et al., 2013), but the fO_2 of magmas related to ore-bearing and barren porphyry intrusions, and the factors controlling the oxygen fugacity of magmas are still not well understood (Hou et al., 2003a; Bi et al., 2006; Liang et al., 2006a,b; Zhang et al., 2013). It is therefore important to examine the principal controls on the oxygen fugacity of these types of magmas in intra-continental settings.

There are several methods for determining the oxygen fugacity of magmas (Wones and Eugster, 1965; Huebner and Sato, 1970; Chou, 1978; Sack et al., 1980; Kilinc et al., 1983; Wones, 1989; Carmichael and Ghiorso, 1986; Wallace and Carmichael, 1994; Metrich and Clocchiatti, 1996; Ballard et al., 2002; Audetat et al., 2004; Stern et al., 2007). Oxygen barometers based on Fe–Ti oxides are easily affected by slow cooling of the magma, and empirical redox indicators such as Fe^{3+}/Fe^{2+} ratios of whole-rock, amphibole and biotite, and the presence of anhydrite rarely survive the processes of hydrothermal alteration and surficial weathering (Ballard et al., 2002). Ce^{4+}/Ce^{3+} ratios of zircon have been shown to be suitable in constraining the relative redox states of magmas (Ballard et al., 2002; Liang et al., 2006a,b). Zircon is a widespread mineral in many types of rocks, and is resistant to strong physical–chemical destruction after crystallization (Lee et al., 1997; Cherniak and Watson, 2001). Ce^{4+}/Ce^{3+} ratios of zircon are controlled by fO_2 of magmas, and not affected by temperature of crystallization (Ballard et al., 2002). For these reasons, the Ce^{4+}/Ce^{3+} ratio of zircon provides a very robust indicator of redox conditions.

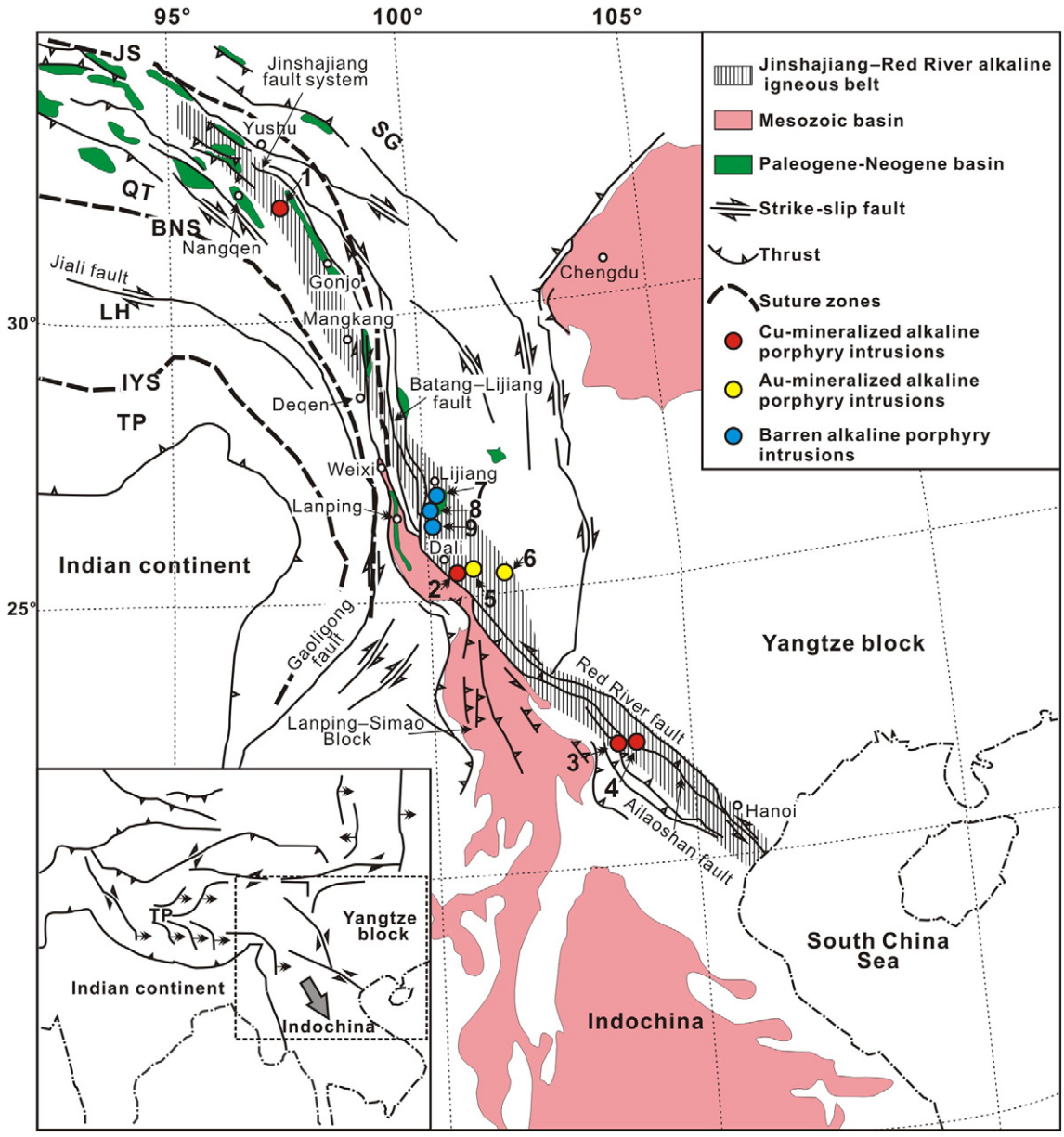

Fig. 1. A simplified geological map of the Jinshajiang–Red River alkaline igneous belt showing the representative Cu-mineralized, Au-mineralized and barren alkaline porphyry intrusions (modified from Wang et al., 2001). Abbreviations: SG—Songpan–Ganze terrane, QT—Qiangtang terrane, LH—Lhasa terrane, TP—Tibetan plateau, JS—Jinshajiang suture, BNS—Bangonghu–Nujiang suture, and IYS—Indian river–Yalu–Zangbu suture; Alkaline porphyry intrusions: 1—Yulong, 2—Machangqing, 3—Tongchang, 4—Chang'anchong, 5—Rentouqing–Jinchangqing, 6—Yao'an, 7—Liuhe, 8—Songgui and 9—Yanshuiqing.

The Jinshajiang–Red River alkaline igneous belt is located in an intra-continental strike-slip fault zone; it is an important belt of Cenozoic porphyry Cu–Au ore deposits in SW China. The Cu-mineralized, Au-mineralized, and barren porphyry intrusions are widely distributed along the belt (Fig. 1; Hou et al., 2003a, b; Hu et al., 2004; Liang et al., 2006a, b; Bi et al., 2004, 2006, 2009). These porphyries are composed of felsic rocks with high alkali ($K_2O + Na_2O$ usually >8 wt.%) and high potassium ($K_2O/Na_2O > 1$), and belong to shoshonitic or high-K calc-alkaline series (Zhang and Xie, 1997; Chung et al., 1997, 1998). Studies using the Ce^{4+}/Ce^{3+} ratio of zircon and the biotite Fe^{3+}–Fe^{2+}–Mg ternary diagram (Liang et al., 2006a,b; Bi et al., 2006, 2009), indicate that the magmas related to the Yulong and Machangqing Cu deposits and Yao'an Au deposit crystallized from relatively oxidized magmas. We propose that a systematic study of the fO_2 of magmas associated with the Cu-mineralized, Au-mineralized and barren porphyry intrusions in the Jinshajiang–Red River alkaline igneous belt may be useful in understanding intra-continental porphyry Cu–Au mineralization.

In this paper, we report Ce^{4+}/Ce^{3+} ratios of zircon, whole-rock major- and trace-element and Sr–Nd isotope data for the representative Cu-mineralized, Au-mineralized and barren porphyry intrusions from the Jinshajiang–Red River alkaline igneous belt. This information when combined with literature data, provide the basis to establish the oxygen fugacity of the magmas which crystallized to form the porphyry intrusions, and we discuss the main controls on the fO_2 of the magmas.

2. Regional geology

The eastern Indo–Asian collision zone is composed of the Songpan–Ganze, Qiangtang and Lhasa terranes and Yangtze blocks, which were welded together prior to the Cretaceous to form part of the Eurasian continent (Fig. 1; Hu et al., 2004). The Cenozoic Jinshajiang–Red River alkaline igneous belt is located in the eastern Indo–Asian collision zone. This belt is 2000 km long, 50–80 km wide and adjacent to the NNW–NW-trending Jinshajiang–Red River deep fault (Fig. 1; Zhang and Xie, 1997; Chung et al., 1997, 1998). Alkaline porphyry intrusion-associated hydrothermal deposits in this belt, including the Yulong and Machangqing Cu deposits and the Yao'an and Rentouqing–Jinchangqing Au deposits, represent one of the most important Cu–Au associations in SW China (Bi et al., 1999, 2002, 2004, 2005, 2009; Hu et al., 1998, 2004; Gu et al., 2003; Wang et al., 2004; Hou et al., 2006, 2007, 2011; Xu et al., 2012, 2014a,b). The Indo–Asian collision at ~65 Ma created the Tibetan plateau; the collision triggered an intensive eastward extrusion in the Tibetan plateau and surrounding regions facilitated by strike-slip motion along a series of strike-slip faults (e.g., the Jinshajiang–Red River, Jiali, Batang–Lijiang and Gaoligong faults; Fig. 1) (Xu et al., 2012). Strike-slip motion along the Jinshajiang–Red River fault led to lithospheric-scale extension and emplacement of hundreds of alkaline intrusions in the Jinshajiang–Red River alkaline igneous belt (Zhang and Xie, 1997; Chung et al., 1997, 1998; Bi et al., 1999, 2009; Yin and Harrison, 2000; Hou et al., 2006, 2007). These alkaline intrusions have been dated, and zircons yield U–Pb ages ranging from ~43 to 35 Ma (Xu, 2011; Xu et al., 2012). The alkaline intrusions have representative rock compositions ranging from basaltic to trachytic and rhyolitic (Chung et al., 1998), and are characterized by high alkali ($K_2O + Na_2O > 8$ wt.%) and enrichment in potassium relative to sodium ($K_2O/Na_2O > 1$); they belong to a high-K calc-alkaline or shoshonitic series (Zhang and Xie, 1997; Chung et al., 1998). Furthermore, the alkaline intrusions show incompatible trace-element patterns which are enriched in large-ion lithophile elements and light rare-earth elements, and the patterns are depleted in high field strength elements such as Nb, Ta and Ti (Chung et al., 1998; Hou et al., 2003b; Bi et al., 2005, 2009). These alkaline intrusions have high I_{sr} and low $\varepsilon_{(Nd)}t$ isotopic compositions, and they were considered to be derived from an enriched mantle source (EMII) (Zhang and Xie, 1997; Hou et al., 2003b; Bi et al., 2005; Jiang et al., 2006).

3. Mineralized and barren porphyry intrusions

Cu-mineralized, Au-mineralized, and barren porphyry intrusions are widely distributed in the Jinshajiang–Red River alkaline igneous belt. Representative Cu-mineralized porphyry intrusions include the Yulong, Machangqing, Tongchang and Chang'anchong. These porphyry intrusions are distributed in the northern, central and southern segments of the Jinshajiang–Red River alkaline igneous belt (Fig. 1). Representative Au-mineralized porphyry intrusions include the Yao'an and Rentouqing–Jinchangqing; they are distributed in the central segment of the Jinshajiang–Red River alkaline igneous belt (Fig. 1). Barren porphyry intrusions include the Liuhe, Songgui and Yanshuiqing in the central part of the Jinshajiang–Red River alkaline igneous belt (Fig. 1).

3.1. Cu-mineralized porphyry intrusions

3.1.1. Yulong

Cu(Mo–Au) mineralization at the Yulong Cu deposit is related to the ~41 Ma monzogranite porphyry stock; this stock has an outcrop area of 0.64 km^2 (Xu et al., 2012), and it intruded the Triassic sandstone and limestone (Fig. 2a; Li et al., 2012). The Yulong monzogranite porphyry intrusions have phenocrysts of K-feldspar, plagioclase, quartz, hornblende and biotite in a cryptocrystalline groundmass (Fig. 3a) with titanite, zircon and apatite as the principal accessory minerals. The Yulong deposit contains over 6.5 Mt Cu with average grades of 0.38 wt.% Cu, 0.04 wt.% Mo, and 0.35 g/t Au (Hou et al., 2003a,b; Liang et al., 2006a; Xu et al., 2012). Alteration zones in the Yulong deposit include the deep K-silicate alteration zone, the shallow quartz–sericite and argillic alteration zones, and the adjacent propylitic alteration zone (Fig. 2a; Hou et al., 2003a,b; Hou et al., 2006; Li et al., 2012). The K-silicate alteration zone, typically developed within the porphyry stock, is characterized by pervasive formation of secondary quartz and K-feldspar. The quartz–sericite alteration zone, formed along the margin of the porphyry stock and typically within the contact, is characterized by alteration of silicate minerals to secondary sericite and quartz. Quartz–sericite alteration overprints the early K-silicate alteration and grades into a more shallow advanced argillic alteration, which is largely composed of kaolinite group minerals and quartz. The propylitic alteration zone, developed in the Triassic sandstone wall-rocks, is characterized by large amounts of chlorite, epidote and tourmaline (Hou et al., 2003a,b). The hydrothermal alteration zones have locally overprinted earlier formed contact metamorphic zones that show a crude zonation from inner hornfels, through to skarn alteration, and marble (Hou et al., 2003a,b; Li et al., 2012). The Yulong deposit is composed of a ring-shaped high-grade Cu–Au mineral zone (about 3 Mt Cu with >1 wt.% Cu and 100 t Au with 4 g/t Au) overlying and surrounding a pipe-like, steeply dipping, veinlet-disseminated Cu–Mo orebody within the monzogranite porphyry stock (Hou et al., 2006).

3.1.2. Machangqing

The Machangqing Cu deposit exhibits Cu(Mo–Au) mineralization within and around the ~35 Ma granite porphyry stock with an outcrop area of 1.3 km^2, and the stock intruded the lower Ordovician and lower Devonian limestone and sandstone (Fig. 2b; Liang et al., 2006b; Xu et al., 2012). The Machangqing granite porphyries have phenocrysts of K-feldspar, plagioclase, quartz, hornblende and biotite in a cryptocrystalline groundmass (Fig. 3b). Titanite, zircon and apatite are the principal accessory minerals. The deposit contains approximately 0.25 Mt Cu at a grade of 0.44 wt.% Cu, 0.03 wt.% Mo and 0.03 g/t Au (Hou et al., 2006). Alteration zones at the Machangqing deposit consist of the deep K-silicate alteration zone, the shallow argillic alteration zone and the adjacent propylitic alteration zone. The K-silicate alteration zone, typically formed within the Machangqing granite porphyry stock, is characterized by pervasive alteration of plagioclase to orthoclase, and of hornblende and primary biotite to secondary biotite. Weak argillic alteration is characterized by the replacement of biotite and feldspar by

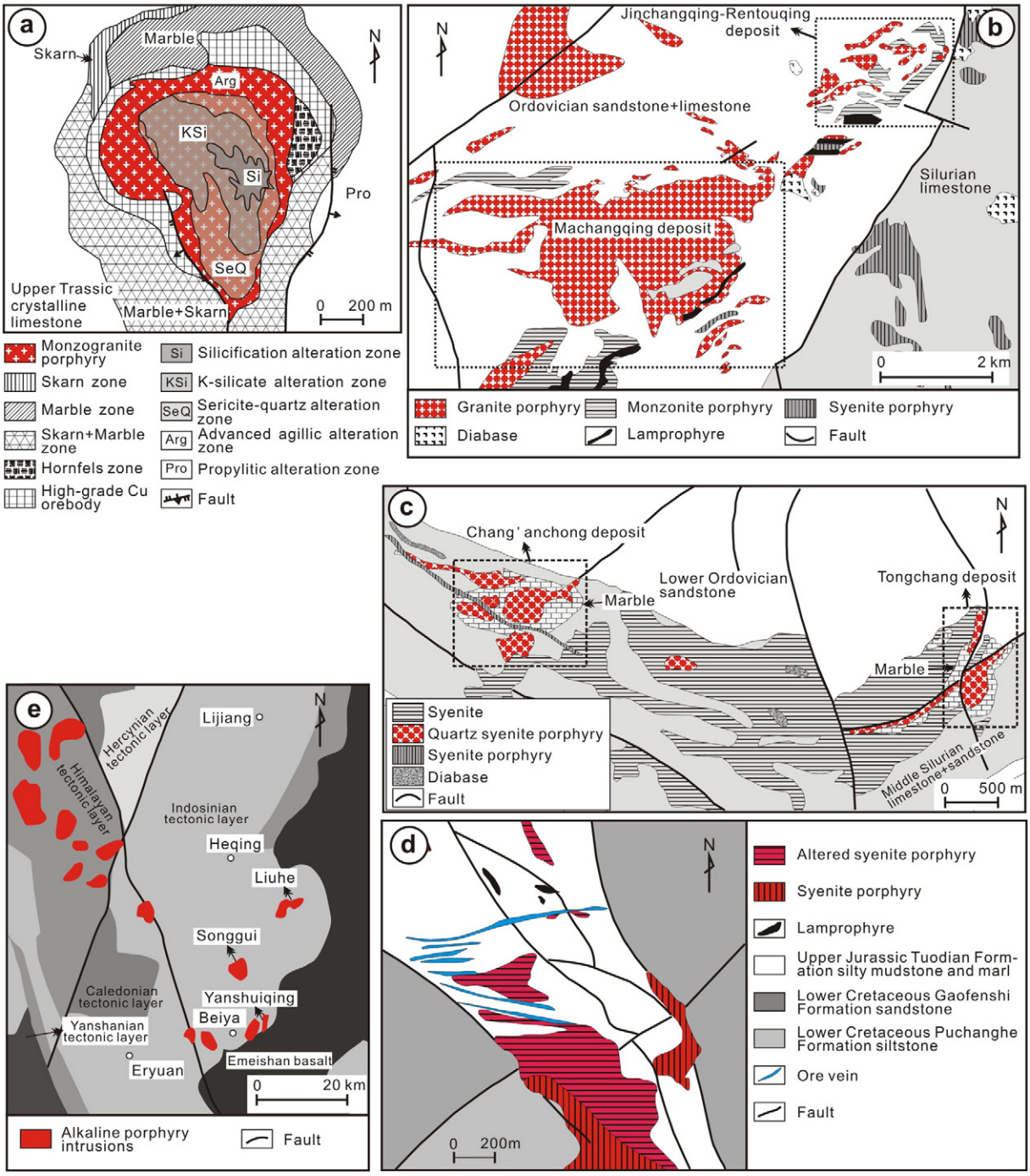

Fig. 2. Simplified geological maps of (a) the Yulong Cu deposit (modified from Hou et al., 2006), (b) Machangqing Cu deposit and Jinchangqing–Rentouqing Au deposit (modified from Li, 2009), (c) Tongchang and Chang'anchong Cu deposits (modified from Xue, 2008), (d) Yao'an Au deposit (modified from Bi et al., 2004), and (e) Liuhe, Songgui and Yanshuiqing alkaline porphyry intrusions (modified from Zhao et al., 2003).

clay minerals. Propylitic alteration is weak but pervasive, forming a wide halo in the country rocks, and the alteration is composed of epidote, chlorite, albite and calcite. The orebodies occur as veins and veinlet–disseminations in the granite porphyry stock, associated with contact hornfels in the lower Ordovician meta-sedimentary rocks, and as skarn mineralization in the Ordovician limestones (Bi et al., 2009). Porphyry-type and skarn-type associations are the two major styles of mineralization at the Machangqing deposit.

3.1.3. Tongchang and Chang'anchong

Both the Tongchang and Chang'anchong deposits contain Cu(Mo–Au) mineralization within and around the ~35 Ma quartz syenite porphyry intrusions (Huang et al., 2009; Xu et al., 2012), which were emplaced into the middle Silurian limestone and sandstone. The intrusion at the Tongchang deposit occurs as stocks and dykes with an outcrop area of 0.2 km^2, and at the Chang'anchong deposit, it occurs as stocks with an outcrop area more than 0.18 km^2 (Fig. 2c; Xu et al., 2012). The Tongchang deposit is located about 5 km east of the Chang'anchong deposit. Tongchang contains 8621 t Cu and 17,060 t Mo with a grade of 1.24 wt.% Cu, 0.218 wt.% Mo and 0.13 g/t Au; the Chang'anchong contains 29,337 t Cu and 13,310 t Mo with a grade of 1.48 wt.% Cu, 0.13 wt.% Mo and 0.25 g/t Au (Xue, 2008). Both the Tongchang and Chang'anchong quartz syenite porphyry intrusions contain rocks with phenocrysts of K-feldspar, plagioclase, quartz,

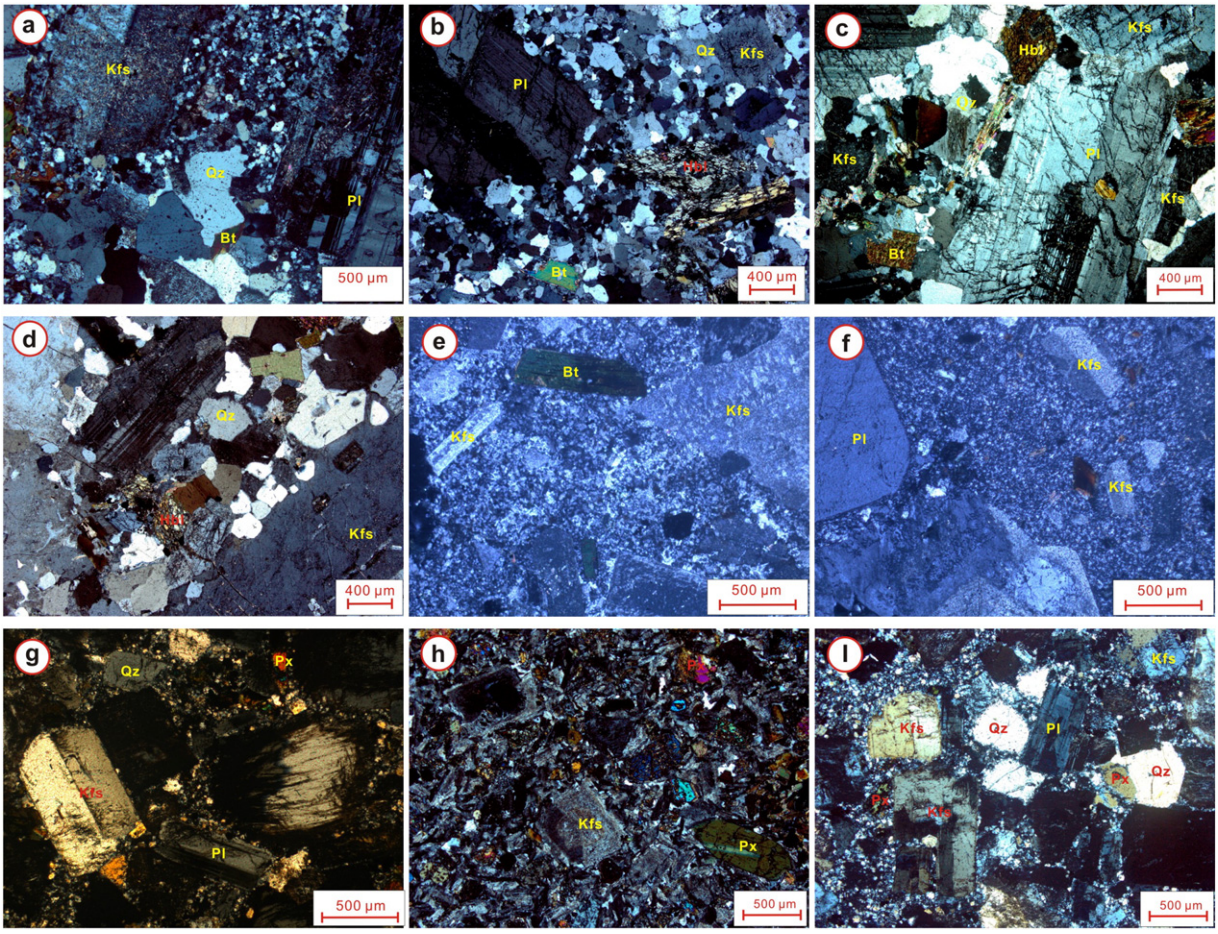

Fig. 3. Photomicrographs showing the textural features and mineral compositions of the Yulong monzongranite porphyries (a), Machangqing granite porphyries (b), Tongchang quartz syenite porphyries (c), Chang'anchong quartz syenite porphyries (d), Yao'an syenite porphyries (e), Rentouqing–Jinchangqing monzonite porphyries (f), Songgui syenite porphyries (g), Liuhe syenite porphyries (h) and Yanshuiqing syenite porphyries (i). Mineral abbreviations: Kfs—K-feldspar, Pl—plagioclase, Qz—quartz, Hbl—hornblende, Bt—biotite, and Px—pyroxene.

hornblende and biotite in a cryptocrystalline groundmass (Figs. 3c–d). Titanite, zircon and apatite are the principal accessory minerals. Quartz syenite porphyry intrusions may originate from a shared source or magma chamber; this is supported by the similar mineral assemblage, whole-rock major- and trace-element data and initial Sr–Nd isotope compositions, and zircon U–Pb age data (Xu, 2011). The mineralized quartz syenite porphyry intrusions at Tongchang and Chang'anchong have similar alteration assemblages and styles of mineralization. Three notable alteration zones (i.e., inner alteration zone, skarn zone and outer alteration zone) have been identified from the inner part of the porphyry intrusion through the contact to the wall-rock, respectively (No. 15 Geological Survey Team (GST) of Yunan Geological Bureau, 1973). The inner alteration zone, exhibiting common alteration and mineralization characteristics for a porphyry Cu–Mo system, is shown by the K-silicate and quartz–sericite alteration of the porphyry intrusion, generally accompanied by abundant spot- and veinlet-disseminated molybdenite and relatively minor veinlet-disseminated chalcopyrite mineralization. The skarn zone, in the contact between the porphyry intrusion and the middle Silurian limestone and sandstone wall-rocks, is characterized by garnet, scapolite, tremolite, epidote, diopside and forsterite, and is generally accompanied by abundant massive and disseminated Cu-sulfide and massive magnetite mineralization. The outer alteration zone within the wall-rocks is mainly composed of marble, with local serpentine, quartz, chlorite, wollastonite and clinohumite; this alteration zone contains local weak Pb–Zn and Cu–Mo mineralization near the skarn zone (No. 15 GST of Yunan Geological Bureau, 1973; Xu et al., 2014a).

3.2. Au-mineralized porphyry intrusions

3.2.1. Yao'an

The Yao'an Au deposit has Au mineralization primarily within and around the ~34 Ma syenite porphyry intrusions with an outcrop area less than 1.0 km^2; the intrusions occur as stocks and apophyses, and were emplaced into the Jurassic silty mudstones and marl (Fig. 2d; Bi et al., 2004, 2009; Lu et al., 2013). The Yao'an syenite porphyries have phenocrysts of K-feldspar, plagioclase, hornblende and biotite in a cryptocrystalline groundmass (Fig. 3e) with the principal accessory minerals of titanite, zircon and apatite. The Yao'an deposit contains ~10 t Au with a grade of 4–5 g/t Au (Bi et al., 2009). The mineralized syenite porphyry intrusions show different degrees of hydrothermal alteration including K-feldspar alteration, sericitization and propylitization (Bi et al., 2009). Close to the orebody, the syenite porphyry intrusion was heavily altered and is characterized by abundant secondary K-feldspar, whereas, away from the orebody, the syenite porphyry intrusion exhibits weak alteration and is characterized by minor calcite as a product of hydrothermal alteration (Bi et al., 2009).

3.2.2. Rentouqing–Jinchangqing

The Rentouqing–Jinchangqing Au deposit is adjacent to the Machangqing Cu deposit (Fig. 2b). The Rentouqing–Jinchangqing deposit contains Au mineralization within the ~36 Ma monzonite porphyry intrusions, and the lower Ordovician and lower Devonian sandstone wall-rocks. The Rentouqing–Jinchangqing monzonite

porphyry intrusions occur as small stocks and dykes with an outcrop area less than 1.0 km^2, and were intruded into the lower Ordovician and lower Devonian limestone and sandstone (Fig. 2b; Xue, 2008; Xu, 2011). The Rentouqing–Jinchangqing monzonite porphyries have phenocrysts of K-feldspar, plagioclase, quartz and biotite in a cryptocrystalline groundmass (Fig. 3f). The principal accessory minerals include titanite, zircon and apatite. The Rentouqing–Jinchangqing deposit consists of two mineral zones: the Rentouqing mineral zone to the west and the Jinchangqing mineral zone to the east, which contain 0.44 t Au at a grade of 5.68 g/t Au, and 5.53 t Au at a grade of 8.73 g/t Au, respectively (Xue, 2008). The fracture zones which were developed in the monzonite porphyry intrusions and wall-rocks are the principal ore-controlling and ore-bearing structures. Gold mineralization was closely related to silicification, pyritization, and arsenopyritization.

3.3. Barren porphyry intrusions

The Yanshuiqing, Songgui and Liuhe barren syenite porphyry intrusions are located between Dali in the south and Lijiang in the north. These porphyry intrusions were intruded into the Caledonian to Himalayan tectonic layers, and occur as stocks and dykes that outcrop in areas of ~15 km^2, ~25 km^2 and ~25 km^2, respectively (Fig. 2e; Xu et al., 2014b). Both the Yanshuiqing and Songgui syenite porphyries have phenocrysts of K-feldspar, plagioclase, pyroxene, quartz, and minor hornblende in a cryptocrystalline groundmass (Figs. 3g–i). The Yanshuiqing and Songgui syenite porphyries have been dated (zircon U–Pb) at ~37 Ma and ~39 Ma, respectively (Xu, 2011). The ~37 Ma Liuhe syenite porphyries (Xia et al., 2005; Xu, 2011) have phenocrysts of K-feldspar, plagioclase and pyroxene, and minor biotite and hornblende in a cryptocrystalline groundmass (Fig. 3h). Titanite, zircon and apatite are the principal accessory minerals in the Yanshuiqing, Songgui and Liuhe syenite porphyry intrusions. The Liuhe syenite porphyry intrusions contain various xenoliths which are composed mainly of the garnet diopside gneiss and garnet diopside amphibolite, and were considered to be derived primarily from the lower crust (Zhao et al., 2003).

4. Sampling and analytical methods

4.1. Trace elements of zircon

Ten rock samples were collected for zircon separation; these samples are from the Cu-mineralized porphyry intrusions (Yulong, Machangqing, Tongchang and Chang'anchong), Au-mineralized porphyry intrusions (Yao'an and Rentouqing–Jinchangqing) and barren porphyry intrusions (Songgui, Liuhe and Yanshuiqing), respectively (Fig. 1). Zircons were separated from a ~2 kg rock sample through standard density and magnetic separation techniques. Representative grains were hand-picked and mounted in an epoxy resin disk, and then polished. Internal structures of zircons were examined using cathodoluminescence (CL) prior to trace-element analysis. CL imaging was obtained using a Quanta 400FEG environmental scanning electron microscope equipped with an Oxford energy dispersive spectroscopy system and a Gatan CL3 + detector at the State Key Laboratory of Continental Dynamics, Northwest University, Xi'an, China. The operating conditions for the CL imaging were 15 kV and 20 nA.

Trace elements of zircon were determined using the laser-ablation, inductively coupled plasma mass spectrometer (LA–ICP–MS) at the State Key Laboratory of Geological Processes and Mineral Resources, China University of Geosciences (Wuhan), China. A pulsed (Geolas) 193 nm ArF Excimer (Lambda Physik, Göttingen Germany) laser power of 50 mJ/pulse energy was used for ablation with diameter of laser spot of 32 μm, at a repetition rate of 10 Hz. Detailed analytical procedures follow those described by Liu et al. (2008, 2010a,b). Helium was used as a carrier gas and argon as the take-up gas, and mixed with the carrier gas via a T-connector before entering the ICP. Zircon standard 91500 was used as a calibration standard for mass discrimination and isotope fractionation and NIST SRM 610 glass as an external standard for trace elements. An Agilent 7500a ICP–MS was used to acquire ion-signal intensities. Each analysis incorporated a background acquisition of approximately 20–30 s (gas blank) followed by 50 s data acquisition from the sample. Off-line selection and integration of background and analytical signals, and time-drift correction and quantitative calibration for zircon trace elements were made using the ICPMSDataCal program (Liu et al., 2010a,b).

4.2. Whole-rock major- and trace-element analyses

Whole-rock major elements were analyzed with a PANalytical Axios—advance (Axios PW4400) X-ray fluorescence spectrometer (XRF) at the State Key Laboratory of Ore Deposit Geochemistry (SKLOG), Institute of Geochemistry, Chinese Academy of Sciences (IGCAS). Fused glass disks were analyzed and the analytical precision as determined on the Chinese National standard GSR-1 and GSR-3 was better than 5%. Loss on ignition (LOI) was obtained using 1 g powder heated up to 1100 °C for 1 h.

Whole-rock trace elements were determined using a Perkin-Elmer ELAN-DRC-e inductively -coupled plasma mass spectrometer (ICP–MS) at the SKLOG. The powdered samples (50 mg) were dissolved in high-pressure Teflon bombs using HF + HNO_3 mixture for 48 h at ~195 °C (Qi et al., 2000). Rhodium was used as an internal standard to monitor signal drift during counting. The international standards GBPG-1 and OU-6, and the Chinese National standard GSR-1 were used for quality control. The analytical precision is 5% or better.

4.3. Whole-rock Sr–Nd isotopic analyses

Whole-rock samples for Sr–Nd isotopic analyses were spiked and dissolved in Teflon bombs with HF + HNO_3 acid, and separated by conventional cation-exchange techniques. The isotopic measurements were performed on a Thermal ionization mass spectrometry—TIMS at the State Key Laboratory of Ore Deposit Geochemistry (SKLOG), Institute of Geochemistry, Chinese Academy of Sciences (IGCAS). The

Table 1
Average trace-element results (ppm) for zircon samples from the Cu-mineralized, Au-mineralized and barren porphyry intrusions in the Jinshajiang–Red River alkaline igneous belt.

Mineralization	Porphyry intrusion	Sample	La	Ce	Pr	Nd	Sm	Eu	Gd	Tb	Dy	Ho	Er	Tm	Yb	Lu	Hf	U	Th
Cu-mineralized	Yulong	YL912 (n = 23)	0.879	56.9	0.317	2.62	3.62	1.57	17.1	5.10	57.2	21.6	102	23.5	244	53.7	9908	1206	651
	Machangqing	BXC920 (n = 21)	0.445	45.1	0.169	1.60	2.65	1.12	14.7	4.90	58.7	23.4	117	28.3	302	66.0	10,743	946	489
		LDS906 (n = 20)	0.686	58.8	0.287	2.69	4.37	1.80	21.7	6.72	76.2	28.3	131	29.6	298	62.4	10,313	1013	660
	Tongchang	TC917 (n = 24)	0.368	49.1	0.185	2.09	3.92	1.69	19.1	6.15	69.5	25.9	121	27.7	281	59.2	9581	1002	502
	Chang'anchong	CA907 (n = 22)	0.584	55.0	0.250	2.49	4.23	1.90	20.7	6.49	73.2	27.0	125	28.5	290	62.2	9734	1067	603
Au-mineralized	Yao'an	YA11-4 (n = 23)	0.118	116	0.280	4.42	7.22	3.25	28.5	7.87	75.1	28.5	114	29.1	241	61.0	8218	1072	1275
	Rentouqing–Jinchangqing	RTQ920 (n = 19)	0.912	48.1	0.318	2.29	3.20	1.31	16.2	5.26	61.2	23.7	113	26.0	266	58.3	10,685	905	520
Barren	Liuhe	LH04 (n = 6)	0.030	11.1	0.131	2.06	4.01	2.75	19.8	6.04	55.9	17.7	60.6	12.1	91.0	19.5	9403	389	134
	Songgui	SG05 (n = 10)	2.63	29.3	1.83	10.8	6.11	2.83	19.4	5.68	60.7	21.6	96.8	21.5	214	44.9	10,393	865	408
	Yanshuiqing	YS01 (n = 7)	0.999	34.3	0.726	6.10	6.88	3.70	27.0	8.24	89.9	32.5	146	32.0	312	64.2	9191	736	694

n in parentheses representing the number of analyzed valid spots in every zircon sample.

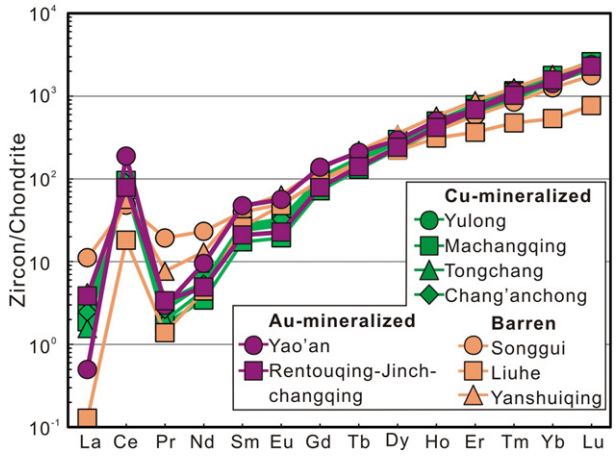

Fig. 4. Chondrite-normalized average zircon REE patterns for the studied alkaline porphyry intrusions (normalization values from Sun and Mcdoonough, 1989).

measured $^{87}Sr/^{86}Sr$ and $^{143}Nd/^{144}Nd$ ratios are normalized to $^{86}Sr/^{88}Sr = 0.1194$ and $^{146}Nd/^{144}Nd = 0.7219$, respectively. The $^{87}Sr/^{86}Sr$ ratio of the NIST SRM987 Sr standard and the $^{143}Nd/^{144}Nd$ ratio of the La Jolla Nd standard solution determined during this study were $^{87}Sr/^{86}Sr = 0.710259 \pm 8$ (2σ, n = 41) and $^{143}Nd/^{144}Nd = 0.511841 \pm 4$ (2σ, n = 53), respectively.

5. Results

5.1. Trace elements, Ce^{4+}/Ce^{3+} ratios and Eu/Eu* values of zircon

Trace-element results for zircon are presented in Table 1 and plotted in Fig. 4. Zircon grains from the Cu-mineralized and Au-mineralized porphyry intrusions are euhedral with clear magmatic oscillatory zoning, and range in diameter from ~150 to 300 μm (Figs. 5a–g); these zircons generally produced consistent trace-element compositions and related U–Pb ages. However, those zircons from the barren porphyry intrusions are relatively small, and subhedral to euhedral with poorly developed magmatic oscillatory zoning (Figs. 5h–j). Many of the analyzed zircon grains from the barren porphyry intrusions yielded complicated trace-element compositions and related complicated U–Pb ages, which probably reflect inheritance of the zircon. Thus, the trace element geochemistry and geochronology data for inherited zircons have been removed.

Chondrite-normalized REE patterns of zircon are characterized by enrichment in HREEs and depletion in LREEs with notably positive Ce anomalies and weak negative Eu anomalies. Ce^{4+}/Ce^{3+} ratios and Eu/Eu* values of zircon were calculated using the method of Ballard et al. (2002) and the data are presented in Table 2. Zircons from the Cu–Au ore-bearing porphyry intrusions have Ce^{4+}/Ce^{3+} ratios from 161 to 265 with an average of 210, whereas the barren porphyry intrusions contain zircons with Ce^{4+}/Ce^{3+} ratios ranging from 9.52 to 33.1 with an average of 24.2. Ce^{4+}/Ce^{3+} ratios of zircon from the Cu–Au

Fig. 5. Cathodoluminescence (CL) images showing the textural features of representative zircon grains from the Yulong (a), Machangqing (b, c), Tongchang (d), Chang'anchong (e), Yao'an (f), Rentouqing–Jinchangqing (g), Liuhe (h), Songgui (i) and Yanshuiqing (j) porphyry intrusions.

ore-bearing porphyry intrusions are notably different from, and much higher than those for the barren porphyry intrusions (Fig. 6a). In contrast, zircons from the Cu–Au ore-bearing porphyry intrusions have Eu/Eu* values varying from 0.55 to 0.69 with an average of 0.60, which are notably lower than those for the barren porphyry intrusions (Eu/Eu* values of zircon = 0.79–0.94, average 0.86) (Fig. 6b).

5.2. Whole-rock major and trace element data

Over 100 rock samples were collected from the Cu-mineralized, Au-mineralized and barren porphyry intrusions, and they have been analyzed for major- and trace-element compositions. The analytical data together with selected previously published data are compiled and presented in Supplementary Tables 1 and 2.

The rocks have a wide range for SiO_2 contents (58.51–72.81 wt.%), and plot into the monzonite, syenite, quartz monzonite and granite fields on the TAS diagram (Fig. 7a). They have elevated alkaline contents ($K_2O + Na_2O$ = 7.45–11.14 wt.%, average 9.37 wt.%) and they show potassium enrichment (K_2O/Na_2O = 0.88–4.53, average 1.53); these rocks can be classified as the products of high-K calc-alkaline and shoshonitic magmatic series (Fig. 7b). On the A/CNK vs. A/NK diagram, these rocks plot in the metaluminous to peraluminous fields (Fig. 7c).

Chondrite-normalized REE patterns of the rock samples are notably enriched in LREEs relative to HREEs (LREE/HREE = 6.94–39.7, average 19.5), and have weakly negative Eu anomalies (Eu/Eu* = 0.47–1.07, average 0.83) (Fig. 8a). Samples from the Cu-mineralized and Au-mineralized porphyry intrusions have higher LREE/HREE ratios (LREE/HREE = 14.0–28.0, average 21.1 versus LREE/HREE = 20.7–39.7, average 30.0) than those from the barren porphyry intrusions (LREE/HREE = 6.94–13.1, average 10.6) (Fig. 8a). Primitive mantle-normalized trace-element patterns of all the samples are relatively enriched in Rb, Ba, Th, U and Pb, and significantly depleted in Nb, Ta, P and Ti (Fig. 8b).

5.3. Whole-rock Sr–Nd isotopic compositions

Newly determined and selected previously published Sr and Nd isotope data for the studied porphyry intrusions are presented in Supplementary Table 3 and plotted in Fig. 9. All the samples exhibit high $(^{87}Sr/^{86}Sr)_i$ and low $\varepsilon_{Nd}(t)$ values, that follow an enriched trend. Plots of the Cu–Au ore-bearing porphyry samples exhibit a linear trend with $(^{87}Sr/^{86}Sr)_i$ values varying from 0.706469 to 0.709314 and $\varepsilon_{Nd}(t)$ values varying from −10.6 to −1.9. However, plots of the barren porphyry samples are relatively concentrated with $(^{87}Sr/^{86}Sr)_i$ values of 0.707094–0.707830 and $\varepsilon_{Nd}(t)$ values of −5.3 to −3.7. Samples from the Cu–Au ore-bearing porphyry intrusions have two-stage depleted mantle model ages (T_{2DM}) of 1706–1003 Ma, whereas samples from the barren porphyry intrusions have two-stage depleted mantle model ages (T_{2DM}) of 1284–1154 Ma.

6. Discussion

6.1. Redox states of the magmas forming the porphyry intrusions

As mentioned above, a remarkable difference in Ce^{4+}/Ce^{3+} ratios of zircon exists between the Cu–Au ore-bearing and barren porphyry intrusions. Ce^{4+}/Ce^{3+} ratios of zircon from the Cu–Au ore-bearing porphyry intrusions are much higher than those for the barren porphyry intrusions. This indicates that the Cu–Au ore-bearing porphyry intrusions have higher fO_2 of magmas than that for the barren porphyry intrusions, which is consistent with conclusions made on the basis of compositions of titanites from these porphyry intrusions (Xu et al., 2014b). The Ce^{4+}/Ce^{3+} ratios of zircon from the Cu–Au ore-bearing porphyry intrusions have a wide range (161 to 265), indicating that magmas with $Ce^{4+}/Ce^{3+} > 161$ (in zircon) have potential to produce intra-continental porphyry Cu–Au mineralization in the Jinshajiang–Red River alkaline igneous belt. This ratio must reach at least 300 in arc settings (Ballard et al., 2002). Without fractional crystallization of plagioclase, the Eu/Eu* value of zircon will positively correlate with the corresponding Ce^{4+}/Ce^{3+} ratio, and in this case the Eu/Eu* value can also indicate redox state of a magma (Ballard et al., 2002). However, in this study, such positive correlations do not exist (Fig. 6b), demonstrating a strong fractional crystallization control from plagioclase in

Table 2
Calculated Ce^{4+}/Ce^{3+} ratios for zircon samples from the Cu-mineralized, Au-mineralized and barren porphyry intrusions in the Jinshajiang–Red River alkaline igneous belt.

Mineralization	Porphyry intrusion	Sample	Zircon Ce^{4+}/Ce^{3+} ratio	Zircon Eu/Eu* value
Cu-mineralized	Yulong	YL912	185	0.61
	Machangqing	LDS906	175	0.55
		BXC920	265	0.57
	Tongchang	TC917	243	0.60
	Chang'anchong	CA907	192	0.62
Au-mineralized	Yao'an	YA11-4	247	0.69
	Rentouqing–Jinchangqing	RTQ920	161	0.56
Barren	Liuhe	LH04	33.1	0.94
	Songggui	SG05	9.52	0.79
	Yanshuiqing	YS01	30.1	0.83

$Eu/Eu^* = \frac{Eu_N}{\sqrt{Sm_N \times Gd_N}}$.

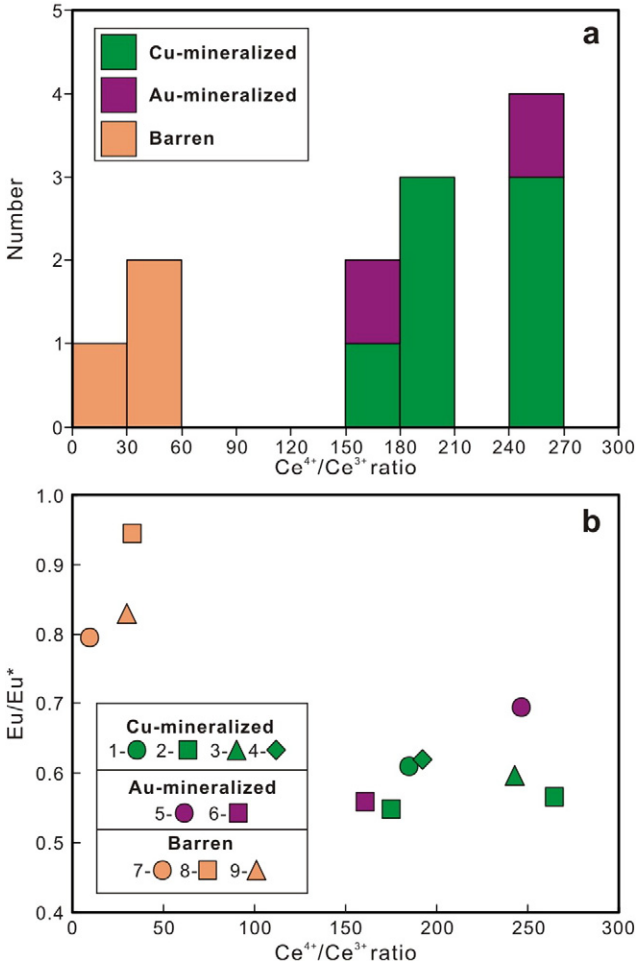

Fig. 6. Histogram of Ce^{4+}/Ce^{3+} ratios of zircon for the studied alkaline porphyry intrusions (a) (selected partial data from Liang et al., 2006a, b), and Ce^{4+}/Ce^{3+} ratios vs. Eu/Eu* of zircon for the studied alkaline porphyry intrusions (b) (symbols: 1—Yulong, 2—Machangqing, 3—Tongchang, 4—Chang'anchong, 5—Yao'an, 6—Rentouqing–Jinchangqing, 7—Liuhe, 8—Songgui, and 9—Yanshuiqing; symbols of the studied alkaline porphyry intrusions in the following figures are the same as those in this figure).

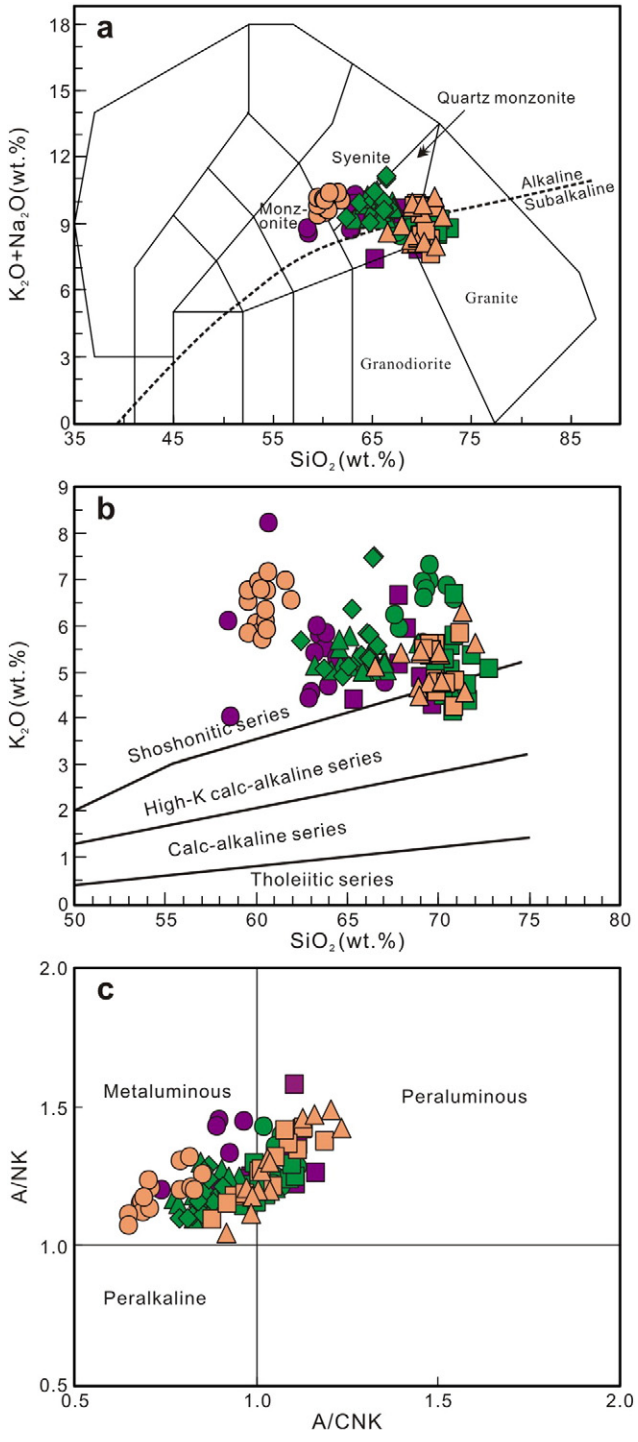

Fig. 7. TAS (a), SiO_2 vs. K_2O (b) and A/CNK vs. A/NK (c) diagrams for the studied alkaline porphyry intrusions.

the Cu–Au ore-bearing magmas, which is supported by other studies (e.g., Xu et al., 2014b).

6.2. Sources of the Cu–Au ore-bearing and barren porphyry intrusions

The sub-continental lithospheric mantle that was modified by hydrous fluids from a subducted Paleo-Tethyan oceanic slab (Zhang and Xie, 1997; Deng et al., 1998a,b; Hou et al., 2003a,b; Bi et al., 2005; Jiang et al., 2006; Xu et al., 2011), thickened juvenile mafic lower crust (Hou et al., 2007, 2011) and juvenile arc lower crust (Li et al., 2012) were previously proposed to be as the sources of the Jinshajiang–Red River alkaline igneous rocks.

Almost all of the alkaline igneous rocks from the Jinshajiang–Red River alkaline igneous belt were emplaced at ~40–30 Ma, and have chemical compositions varying from basaltic to trachytic and rhyolitic (Zhang and Xie, 1997; Chung et al., 1998); these rocks have similar Sr–Nd isotopes, trace-element and REE patterns, $K_2O + Na_2O$ and K_2O/Na_2O (Zhang and Xie, 1997; Chung et al., 1997, 1998). Moreover, coeval alkaline mafic and ultramafic rocks in the belt display geochemical characteristics similar to intermediate-acidic rocks in the same belt (Xie and Zhang, 1995; Deng et al., 1998a, b; Guan et al., 2006; Dong et al., 2007); this indicates that the alkaline igneous rocks in the Jinshajiang–Red River alkaline igneous belt could not be directly derived from the thickened juvenile mafic lower crust or juvenile arc lower crust, but most possibly from an enriched metasomatized mantle sources (EMII-type mantle) as revealed by the high $(^{87}Sr/^{86}Sr)_i$ values and low $\varepsilon_{Nd}(t)$ values (Fig. 9; Zhang and Xie, 1997; Deng et al., 1998a, b; Hou et al., 2003a, 2003b; Bi et al., 2005; Jiang et al., 2006; Xu et al., 2011).

The Cu–Au ore-bearing and barren alkaline porphyry intrusions (Zhang and Xie, 1997; Chung et al., 1997, 1998) show enrichment of LILEs (such as Rb, Ba and Sr) and LREEs, and depletion of HFSEs (such as Nb, Ta and Ti) (Figs. 8a–b), indicating an arc-magmatic affinity (Figs. 10a–b); this suggests that the Cu–Au ore-bearing and barren alkaline porphyry intrusions were derived from a mantle wedge that was modified by subducted slab-derived fluids (Gill, 1981; Tatsumi et al., 1986; Tatsumi, 1989; Ionov and Hofmann, 1995; Hofmann and Jochum, 1996; Richards, 2003). Some studies indicate that these alkaline porphyry intrusions were not emplaced in an arc-setting, but in

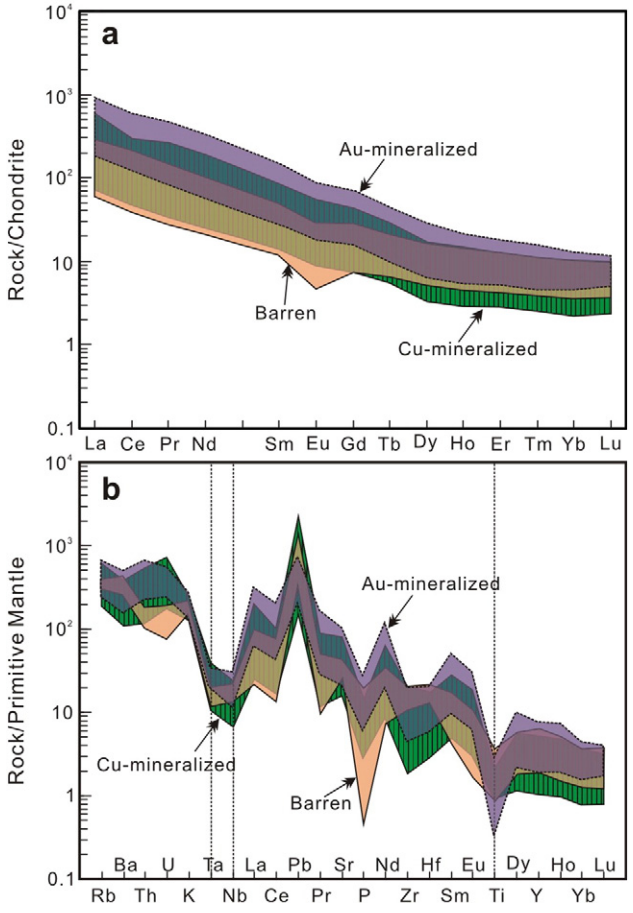

Fig. 8. Chondrite-normalized whole-rock REE diagram (a) and primitive mantle-normalized whole-rock trace-element diagram (b) for the studied alkaline porphyry intrusions (normalization values from Sun and Mcdoonough, 1989).

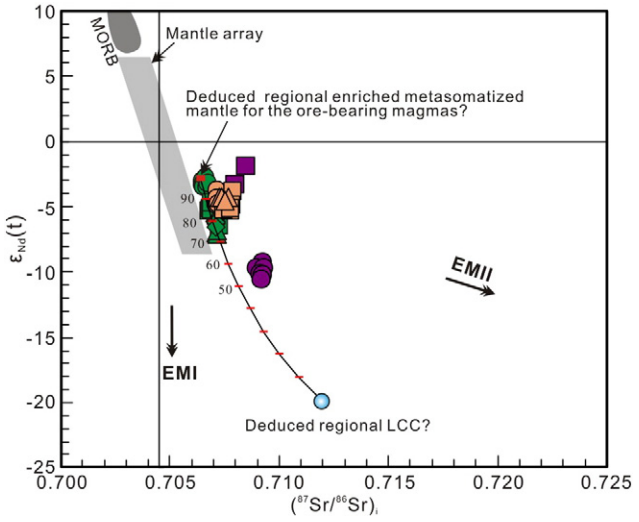

Fig. 9. $(^{87}Sr/^{86}Sr)_i$ vs. $\varepsilon_{Nd}(t)$ diagram for the studied alkaline porphyry intrusions (MORB, mantle array, EMI and EMII trends from Sun and Mcdoonough, 1989). The mixing between regional enriched metasomatized mantle and regional LCC is used to model crustal assimilation degrees of the ore-bearing magmas. The Sr (ppm), Nd (ppm), $(^{87}Sr/^{86}Sr)_i$ and $\varepsilon_{Nd}(t)$ for end members used in mixing calculation: 662, 25.5, 0.7064 and −2.9 for regional enriched metasomatized mantle (estimated from Xie et al., 1999); 300, 24, 0.712 and −20 for regional LCC (estimated from Jahn et al., 1999; Hou et al., 2013).

an intra-continental strike-slip fault zone (Chung et al., 1997; Zhang and Xie, 1997; Hou et al., 2003a,b, 2006, 2007, 2011; Xu et al., 2012). Therefore, to explain the arc-magmatic affinity of these alkaline porphyry intrusions is important. Subduction of the oceanic slab took place between the early Permian and the late Triassic in this region, resulting in the closure of the Jinshajiang–Ailaoshan Paleo-Tethyan oceanic basin (Pan et al., 1996, 2003; Mo and Pan, 2006). Subduction of the Paleo-Tethyan oceanic slab possibly modified the mantle wedges, which were preserved and became the sources of the alkaline magmas. Partial melts of the enriched metasomatized mantle sources (EMII type) gave rise to the alkaline magmas for the Cu–Au ore-bearing and barren porphyry intrusions.

6.3. Process of formation of high fO_2 of magmas associated with porphyry Cu–Au mineralization

High fO_2 of magmas may be generated by the following processes: 1) metasomatism of a mantle source prior to or during partial melting, induced by the subducted slab-derived hydrous fluids or silicate melts with enrichment in oxidation agents such as Fe^{3+}, CO_2 or sulfate (Wyllie, 1978; Tatsumi, 1989; Davies and Stevenson, 1992; Peacock, 1993; McInnes and Cameron, 1994; Brandon and Draper, 1996; Mungall, 2002; Oyarzun et al., 2008), and 2) modification or magmatic evolution after formation of magmas. The second process model includes: (1) fractional crystallization of the Fe^{2+}-bearing silicate, oxide or sulfide phases in a closed-system magma chamber (Carmichael and Ghiorso, 1986), (2) degassing of a hydrous magma at low pressures with preferential removal of reduced volatile species such as H_2 or H_2S (Czamanske and Wones, 1973; Candela, 1986; Ague and Brimhall, 1988), and (3) assimilation of the oxidized country rocks during migration of a magma from depth to higher levels in the crust (Ballard et al., 2002).

There are two main viewpoints for the genesis of the high fO_2 of magmas which are associated with porphyry Cu–Au mineralization: (1) the high fO_2 was caused by K- and Fe-enriched fluids in sources of the magmas (Bi et al., 2006) or caused by H_2O from breakdown of amphibole in sources of the magmas (Hou et al., 2007, 2011), and (2) the high fO_2 was caused primarily by assimilation of the H_2O-rich oxidized crustal components during ascent of the magma from the sources (Liang et al., 2006a,b).

6.3.1. Crustal assimilation and its influence on the redox states of magmas for the Cu–Au ore-bearing and barren porphyry intrusions

Most of the Cu–Au ore-bearing porphyry intrusions have Nb/Ta ratios of 5.8–14.3 with an average of 11.9, which are similar to the values for the continental crust (Nb/Ta = 12–13; Pfänder et al., 2007), but lower than that of average global subduction sediments (Nb/Ta = 14.2; Plank and Langmuir, 1998) and those of the barren porphyry intrusions (Nb/Ta = 15.3–19.6, average 16.9) (Fig. 11a). The exception to this is the Yao'an ore-bearing porphyry intrusion. As HFSEs, Nb and Ta have similar geochemical behavior, and are not fractionated in most magmatic processes (Liang et al., 2009). Ti-rich minerals such as rutile, titanite and ilmenite are the potential minerals that fractionate Nb from Ta (Green, 1995; Dostal and Chatterjee, 2000; Ying et al., 2007); these minerals favor Ta over Nb in the silicate melt (Foley et al., 2000; Horng and Hess, 2000; Schmidt et al., 2004; Klemme et al., 2005; Xiong et al., 2005; Bromiley and Reffern, 2008; Liang et al., 2009). Fractional crystallization of these Ti-rich minerals would lead to an increase of Nb/Ta ratio in the residual melt. However, such a scenario is not observed in the Cu–Au ore-bearing and barren porphyry intrusions (Fig. 11b). Therefore, relative to the barren porphyry intrusions, the lower Nb/Ta ratios of the Cu–Au ore-bearing porphyry intrusions may be caused primarily by crustal assimilation rather than fractional crystallization of Ti-rich minerals. The abundance of Mo

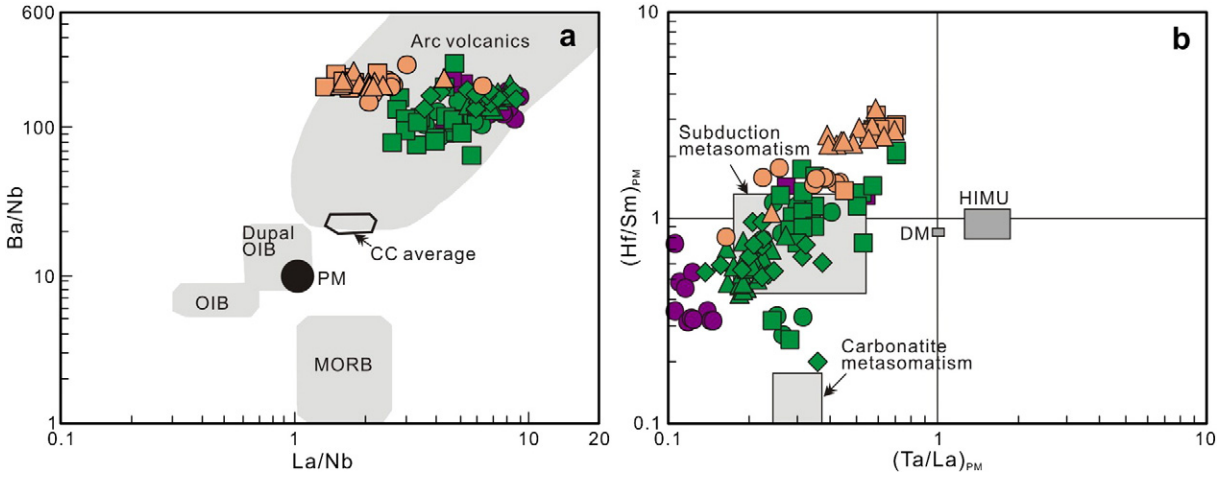

Fig. 10. La/Nb vs. Ba/Nb diagram (a) (MORB, PM, OIB, Dupal OIB, continental crust (CC) average and arc volcanics are from Jahn et al., 1999), and $(Ta/La)_{PM}$ vs. $(Hf/Sm)_{PM}$ diagram (b) (subduction- and carbonatite-related metasomatism from La Flèche et al., 1998; DM and HIMU from Pfänder et al., 2007) for the studied alkaline porphyry intrusions.

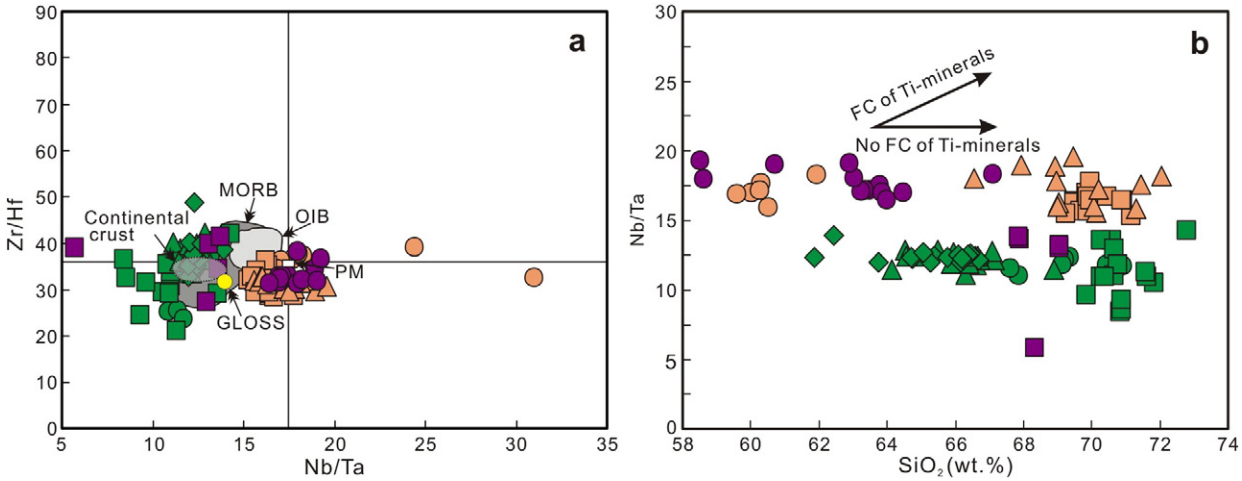

Fig. 11. Nb/Ta vs. Zr/Hf diagram (a) (PM from Sun and Mcdoonough, 1989; GLOSS from Plank and Langmuir, 1998; Others from Pfänder et al., 2007), and SiO_2 vs. Nb/Ta diagram (b) for the studied alkaline porphyry intrusions.

in these porphyry Cu deposits also indicates that these Cu ore-bearing magmas underwent crustal assimilation, because Mo was derived mainly from the crust (Hou et al., 2011; Richards, 2011). $\varepsilon_{Nd}(t)$ values of the Cu–Au ore-bearing porphyry intrusions do not increase with increasing Nd contents (Fig. 12); this indicates that crustal assimilation probably occurred in the shallower level magma chambers of the Cu–Au ore-bearing magmas, not during magma ascent.

Crustal assimilation of the Cu–Au ore-bearing magmas most likely occurred in the "MASH" (i.e., crustal melting and assimilation by primary basaltic magmas, magma storage at the base of the crust, and magma homogenization; Richards, 2003) process, when their basaltic parental magmas that were generated in the enriched metasomatized mantle sources, under-plated at the crust/mantle boundary or near the base of the crust due to density contrasts (Richards, 2003, 2011). Regional enriched metasomatized mantle and regional lower crust as two end-members for mantle–crust mixing which may explain the formation of most of the Cu–Au ore-bearing magmas. Sr–Nd isotopic mixing models indicate that different degrees of crustal assimilation are recorded in the different Cu–Au ore-bearing magmas as revealed by increasing $(^{87}Sr/^{86}Sr)_i$ values and decreasing $\varepsilon_{Nd}(t)$ values (Fig. 9). Increasing two-stage depleted mantle model ages (T_{2DM}) (Supplementary Table 3) with the different Cu–Au ore-bearing magmas further indicate that different degrees of crustal assimilation (possibly representing old lower crust) occurred between the Cu–Au ore-bearing magmas.

Most of the ore-bearing magmas show evidence of crustal contamination, but the Tongchang, Chang'anchong, and Machangqing ore-bearing magmas (which exhibit larger degrees of crustal assimilation than the Yulong and Rentouqing–Jinchangqing ore-bearing magmas) did not form from a high fO_2 magma. Thus, the fO_2 of magmas for the alkaline porphyry intrusions mainly reflected the redox states of the sources. The Cu- and Au-released from sulfides in the sources requires a high-fO_2 condition than the sulfide–sulfur oxide buffer (ΔSSO) or more than two orders of magnitude higher than fayalite–magnetite–quartz oxygen buffer (ΔFMQ + 2) (Mungall, 2002; Richards, 2003, 2011; Sun et al., 2004, 2013). Therefore, the high fO_2 of the Cu–Au ore-bearing magmas in the Jinshajiang–Red River alkaline igneous belt is probably derived from the high fO_2 of the sources, and the fO_2 of magmas for the Cu–Au ore-bearing and barren porphyry intrusions mainly reflected the redox states of the sources. The difference of fO_2 of magmas between the Cu–Au ore-bearing and barren porphyry intrusions might suggest different characteristics of the sources.

6.3.2. Different enrichment mechanisms of the metasomatized mantle sources for mineralized versus barren porphyry intrusions

LILEs and HFSEs have different geochemical behaviors in fluids and melts (Hawkesworth et al., 1997). LILEs, such as Rb, Ba, Sr, K and U, are relatively mobile in fluids released from the subducted slab, whereas it has been suggested that Th, LREEs and HFSEs are mobilized by the melts (Pearce and Peate, 1995; Elliott et al., 1997; Hawkesworth et al.,

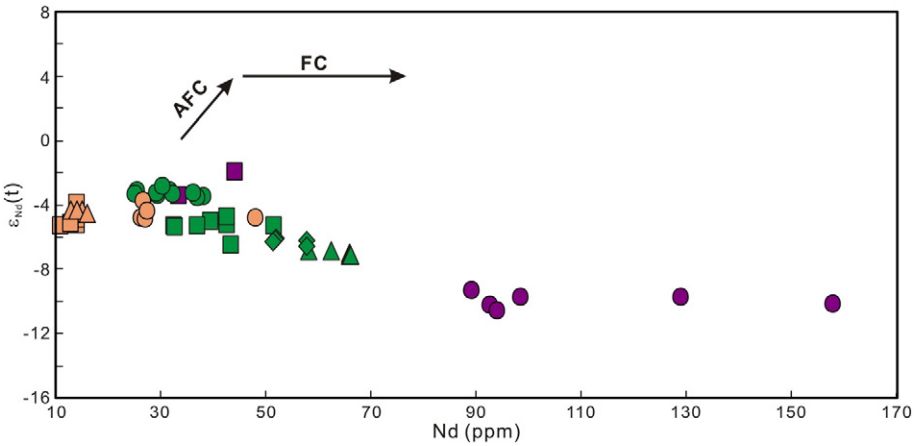

Fig. 12. Nb vs. $\varepsilon_{Nd}(t)$ diagram for the studied alkaline porphyry intrusions.

1997; Class et al., 2000). The clear enrichment of LILEs and LREEs, the depletion of HFSEs (Figs. 8a–b), and the high Ba/Th and Ba/La ratios of the barren porphyry intrusions (Figs. 13a–b), indicate that a source was modified mainly by slab-derived fluids (Pearce and Peate, 1995; Elliott et al., 1997). The Cu–Au ore-bearing porphyry intrusions not only have obvious enrichment of LILEs and LREEs, and depletion of HFSEs (Figs. 8a–b), but also have high Th/Nb and Th/Yb ratios (Figs. 13a–b). This indicates that the source was modified not only by the slab-derived fluids but also by the slab-derived melts (Johnson and Plank, 1999; Class et al., 2000). The sources of the ore-bearing porphyry intrusions of the Dexing porphyry Cu(Mo–Au) deposit and the Gangdese porphyry Cu(Mo) belt, in intra-continental settings, also show enrichment related to slab-derived melts (Figs. 13a–b); this also points to enrichment created by slab-derived melts in the formation of the porphyry Cu–Au mineralization.

The Cu–Au ore-bearing porphyry intrusions in the Jinshajiang–Red River alkaline igneous belt have much higher Th/Nb and Th/Yb ratios than those for the crust and lower continental crust (LCC) (Figs. 13a–b), indicating that influence from crustal assimilation on Th/Nb and Th/Yb ratios for the Cu–Au ore-bearing porphyry intrusions is negligible. The Th/Nb and Th/Yb ratios of the Cu–Au ore-bearing porphyry intrusions in the belt are much higher than those for the average global

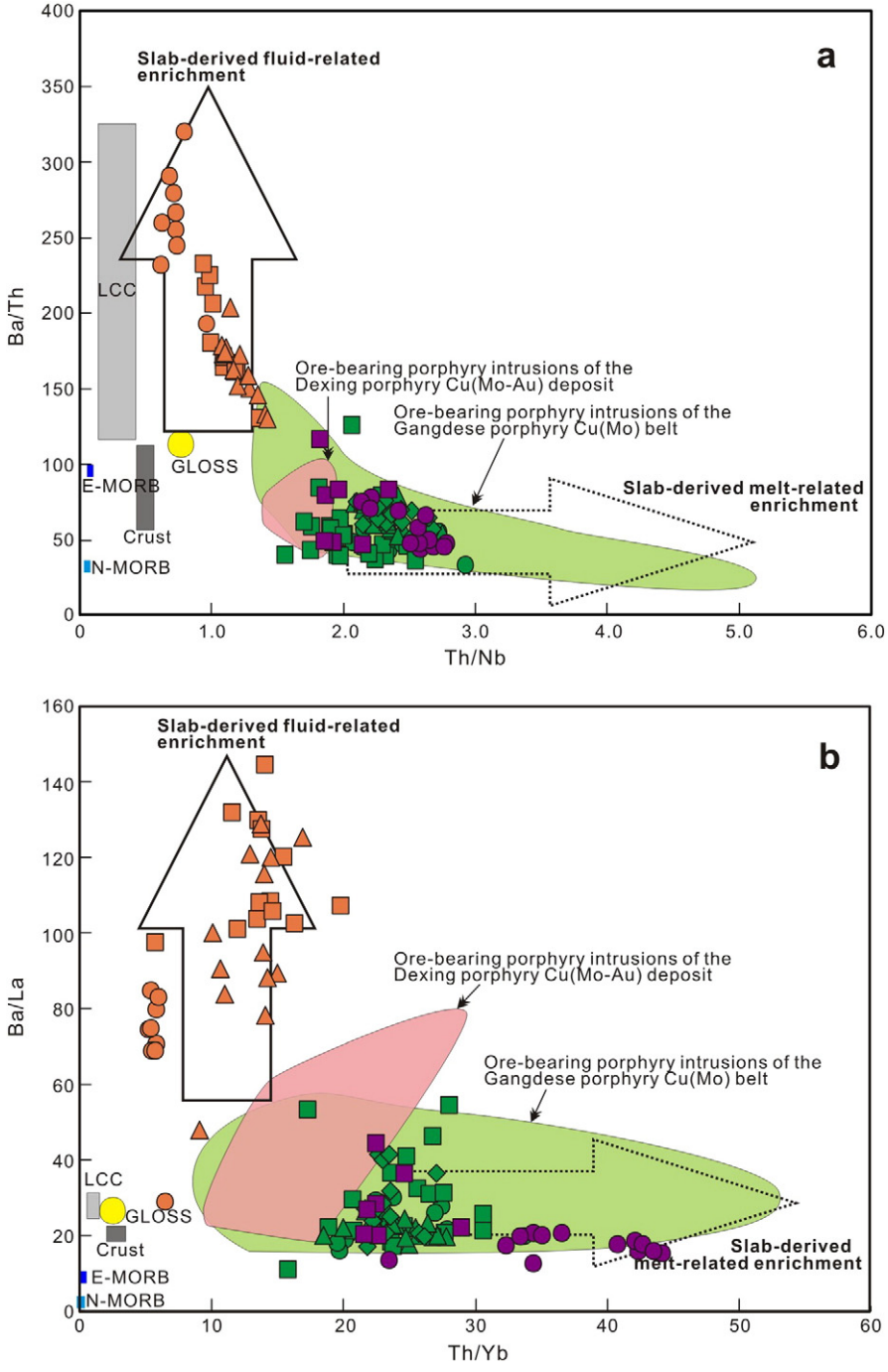

Fig. 13. Th/Nb vs. Ba/Th diagram (a) (after Elliott et al., 1997), and Th/Yb vs. Ba/La diagram (b) (after Dokuz, 2011) for the studied alkaline porphyry intrusions (LCC and Crust from Rudnick and Fountain, 1995; N-MORB and E-MORB from Sun and Mcdoonough, 1989; GLOSS from Plank and Langmuir, 1998; Ore-bearing porphyry intrusions of the Dexing porphyry Cu(Mo–Au) deposit from Liu et al., 2012; Ore-bearing porphyry intrusions of the Gangdese porphyry Cu(Mo) belt from Hou et al., 2004; Zheng et al., 2004; Wang et al., 2006; Xu et al., 2010; Leng et al., 2013).

sediment from subduction zone settings (GLOSS), E-MORB and N-MORB (Figs. 13a–b), which supports the idea that slab-derived melts were responsible for modification of sources of the Cu–Au ore-bearing porphyry intrusions (Hawkesworth et al., 1997; Oyarzun et al., 2008; Dokuz, 2011). The slab-derived melts with high Th/Nb and Th/Yb ratios, which are different from adakitic melts, were most likely derived from low degrees of partial melting of an altered oceanic crust where subducted sediments were incorporated (Hawkesworth et al., 1997; Oyarzun et al., 2008; Dokuz, 2011). Partial melting of the altered oceanic crust with rutile and garnet as the main residual minerals that may sequestrate the majority of the HFSEs and HREEs such as Nb, Ta and Yb, gave rise to a slab-derived melt with high Th/Nb and Th/Yb ratios. Although melting of the oceanic crust requires special conditions, some relatively uncommon scenarios including shallow or stalled subduction where the slab has more time to heat up at shallow depths, ridge subduction, or edge-melting of the detached slabs or slab windows, might result in melting of the subducted oceanic crust (Gao et al., 2010; Richards, 2011, and references therein).

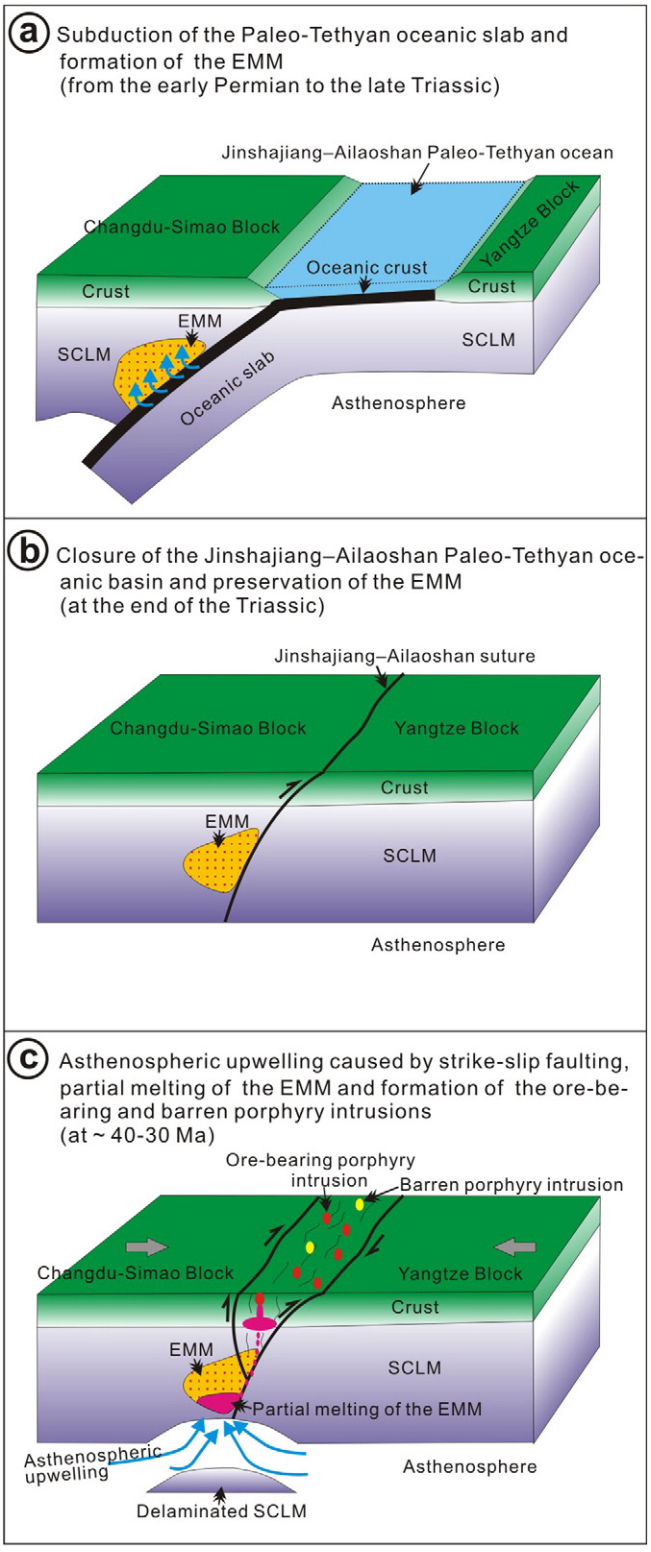

Fig. 14. Schematic model illustrating the various stages to explain genesis of the Cu–Au ore-bearing and barren porphyry intrusions in the Jinshajiang–Red River alkaline igneous belt through the partial melting of the ancient enriched metasomatized mantle sources. Abbreviations: SCLM—sub-continental lithospheric mantle and EMM—enriched metasomatized mantle.

6.3.3. Possible process producing the Cu–Au ore-bearing and barren porphyry intrusions

Elemental and isotope ratio data indicate that the Cu–Au ore-bearing and barren porphyry intrusions were derived from metasomatically enriched mantle sources formed by subduction of a slab of Paleo-Tethyan oceanic crust. A simplified scenario is shown in Fig. 14 to account for the formation of these porphyry intrusions from magmas with different fO_2 within the Jinshajiang–Red River alkaline igneous belt (Fig. 14).

From the early Permian, the Jinshajiang–Ailaoshan Paleo-Tethyan oceanic slab began to subduct westwards beneath the Changdu–Simao block (Fig. 14a; Pan et al., 1996, 2003; Mo and Pan, 2006). During subduction, the hydrous oceanic slab experienced dehydration and partial melting, resulting in formation of the slab-derived fluids and slab-derived melts. Interaction of the slab-derived fluids and slab-derived melts with overlying mantle wedge led to formation of the heterogeneous enriched metasomatized mantle sources (Fig. 14a). The sources of the barren porphyry intrusions were affected mainly by slab-derived fluids, whereas the sources of the Cu–Au ore-bearing porphyry intrusions were modified by both slab-derived fluids and slab-derived melts.

By the end of the Triassic, the closure of the Jinshajiang–Ailaoshan Paleo-Tethyan oceanic basin led to the final collision of the Changdu–Simao and Yangtze blocks (Pan et al., 1996, 2003; Mo and Pan, 2006) and preservation of the enriched metasomatized mantle sources (Fig. 14b).

The Indo–Asian collision at ~65 Ma created the Tibetan plateau, and the collision triggered an intensive eastward extrusion in the Tibetan plateau and surrounding regions; this extrusion was facilitated by strike-slip motion along a series of strike-slip faults such as the Jinshajiang–Red River mantle-penetrating fault. Strike-slip faulting of the Jinshajiang–Red River mantle-penetrating fault caused lithospheric-scale extension and upwelling of the asthenosphere; the heat produced by this process produced partial melts of the ancient enriched metasomatized mantle sources, resulting in the emplacement of the alkaline porphyry intrusions and associated porphyry Cu–Au mineralization in this region at ~40–30 Ma (Fig. 14c; Chung et al., 1997, 1998; Zhang and Xie, 1997; Bi et al., 1999, 2009; Yin and Harrison, 2000; Hou et al., 2006, 2007; Xu et al., 2012).

7. Conclusions

(1) The Cu–Au ore-bearing porphyry intrusions formed from magmas with much higher fO_2 than the melt which produced the barren porphyry intrusions.
(2) The Cu–Au ore-bearing and barren porphyry intrusions were derived from the ancient enriched metasomatized mantle sources (EMII type) formed by subduction of the Paleo-Tethyan oceanic slab.
(3) Most of the Cu–Au ore-bearing magmas experienced crustal assimilation in the "MASH" process; however, this process did not change their original redox states.

(4) The fO_2 of magmas that formed the Cu–Au ore-bearing and barren porphyry intrusions mainly reflected the redox states of their sources, and different fO_2 of magmas for the Cu–Au ore-bearing and barren porphyry intrusions could be ascribed to different enrichment mechanisms of the sources. Sources of the barren porphyry intrusions were affected mainly by the slab-derived fluids, whereas sources of the Cu–Au ore-bearing porphyry intrusions were modified by both the slab-derived fluids and slab-derived melts.

Supplementary data to this article can be found online at http://dx.doi.org/10.1016/j.oregeorev.2015.05.007.

Acknowledgments

This research project is jointly supported by "the Key Natural Science Foundation of China (41130423), the National Natural Science Foundation of China (41203041, 41473052), the 12th Five-Year Plan Project of State Key Laboratory of Ore-deposit Geochemistry, Chinese Academy of Sciences (SKLODG-ZY125-03) and the West Ph.D. project of West Light Foundation of the Chinese Academy of Sciences". The kind help during fieldwork from staff of Yunnan Honghe Henghao Mining Co. Ltd., Yunnan Copper Industry Co. Ltd. and Tibet Yulong Copper Industry Co. Ltd. is gratefully acknowledged. Professor Zhaochu Hu (China University of Geosciences, Wuhan) is thanked for the LA–ICPMS zircon analysis. We are very grateful to Professor Meifu Zhou (Hong Kong University) and two anonymous referees for their constructive advice on the manuscript. Editor in-chief Professor Franco Pirajno and Guest editor Dr Peter C. Lightfoot are also greatly appreciated for their constructive comments and suggestions.

References

Ague, J.J., Brimhall, G.H., 1988. Magmatic arc asymmetry and distribution of anomalous plutonic belts in the batholiths of California: effects of assimilation, crustal thickness, and depth of crystallization. Geol. Soc. Am. Bull. 100, 912–927.

Audetat, A., Pettke, T., Dolejs, D., 2004. Magmatic anhydrite and calcite in the ore-forming quartz–monzodiorite magma at Santa Rita, New Mexico (USA): genetic constraints on porphyry-Cu mineralization. Lithos 72, 147–161.

Ballard, J.R., Palin, J.M., Campbell, I.H., 2002. Relative oxidation states of magmas inferred from Ce(IV)/Ce(III) in zircon: application to porphyry copper deposits of northern Chile. Contrib. Mineral. Petrol. 144, 347–364.

Bi, X.W., Hu, R.Z., Ye, Z.J., Shao, S.X., 1999. Study on the relation between the A-type granite and Cu ore mineralization: evidence from the Machangqing copper deposit. Sci. China (Ser. D) 29, 489–495 (in Chinese).

Bi, X.W., Cornell, D.H., Hu, R.Z., 2002. REE composition of primary and altered feldspar from the mineralized alteration zone of alkali-rich intrusive rocks, western Yunnan Province, China. Ore. Geol. Rev. 19, 69–78.

Bi, X.W., Hu, R.Z., Cornell, D.H., 2004. Trace element and isotope evidence for the evolution of ore-forming fluid of Yao'an gold deposit, Yunnan Province, China. Miner. Depos. 39, 21–30.

Bi, X.W., Hu, R.Z., Peng, J.T., Wu, K.X., Su, W.C., Zhan, X.Z., 2005. Geochemical characteristics of the Yao'an and Machangqing alkaline-rich intrusions. Acta Petrol. Sin. 21, 113–124 (in Chinese with English abstract).

Bi, X.W., Hu, R.Z., Mungall, J., Hanley, J.J., Peng, J.T., Wu, K.X., Li, H.L., 2006. Mineral chemistry studies of Cu- and Au-mineralized alkaline inrusions. Acta Mineral. Sin. 26, 377–386 (in Chinese with English abstract).

Bi, X.W., Hu, R.Z., Hanley, J.J., Mungall, J., Peng, J.T., Shang, L.B., Wu, K.X., Suang, Y., Li, H.L., Hu, X.Y., 2009. Crystallisation conditions (T, P, fO_2) from mineral chemistry of Cu- and Au-mineralised alkaline intrusions in the Red River–Jinshajiang alkaline igneous belt, western Yunnan Province, China. Mineral. Petrol. 96, 43–58.

Brandon, A.D., Draper, D., 1996. Constraints on the origin of the oxidation state of mantle overlying subduction zones: an example from Simcoe, Washington, USA. Geochim. Cosmochim. Acta 60, 1739–1749.

Bromiley, G.D., Reffern, S.A.T., 2008. The role of TiO_2 phases during melting of subduction-modified crust: implications for deep mantle melting. Earth Planet. Sci. Lett. 267, 301–308.

Candela, P.A., 1986. The evolution of vapor from silicate melt: effect on oxygen fugacity. Geochim. Cosmochim. Acta 50, 1205–1211.

Carmichael, I.S.E., Ghiorso, M.S., 1986. Oxidation–reduction relations in basic magma: a case for homogeneous equilibria. Earth Planet. Sci. Lett. 78, 200–210.

Carroll, M.R., Rutherford, M.J., 1987. The stability of igneous anhydrite: experimental results and implications for sulfur behavior in the 1982 El Chichon trachyandesite and other evolved magmas. J. Petrol. 28, 781–801.

Cherniak, D.J., Watson, E.B., 2001. Pb diffusion in zircon. Chem. Geol. 172, 5–24.

Chou, I.M., 1978. Calibration of oxygen buffers at elevated-P and elevated-T using hydrogen fugacity sensor. Am. Mineral. 63, 690–703.

Chung, S.L., Lee, T.Y., Lo, C.H., Wang, P.L., Chen, C.Y., Yem, N.T., Hoa, T.T., Wu, G.Y., 1997. Intraplate extension prior to continental extrusion along the Ailao Shan Red River shear zone. Geology 25, 311–314.

Chung, S.L., Lo, C.H., Lee, T.Y., Zhang, Y.Q., Xie, Y.W., Li, X.H., Wang, K.L., Wang, P.L., 1998. Diachronous uplift of the Tibetan plateau starting 40 Myr ago. Nature 394, 769–773.

Class, C., Miller, D.M., Goldstein, S.L., Langmuir, C.H., 2000. Distinguishing Melt and Fluid Subduction Components in Umnak Volcanics, Aleutian Arc. http://dx.doi.org/10.1029/1999GC000010 (G3 1:1004).

Czamanske, G.K., Wones, D.R., 1973. Oxidation during magmatic differentiation, Finnmarka complex, Oslo area, Norway. Part 2. The mafic silicates. J. Petrol. 14, 349–380.

Davies, J.H., Stevenson, D.J., 1992. Physical model of source region of subduction zone volcanics. J. Geophys. Res. Solid Earth 97, 2037–2070.

Deng, W.M., Huang, X., Zhong, D.L., 1998a. Petrological characteristics and genesis of Cenozoic alkali-rich porphyry in west Yunan, China. Sci. Geol. Sin. 33, 412–425 (in Chinese with English abstract).

Deng, W.M., Huang, X., Zhong, D.L., 1998b. Alkali-rich porphyries in northern segment of Jinshajiang belt in western Yunnan province and their relationship with intraplate distortion. Sci. China (Ser. D) 28, 111–117 (in Chinese).

Dokuz, A., 2011. A slab detachment and delamination model for the generation of Carboniferous high-potassium I-type magmatism in the Eastern Pontides, NE Turkey: the Ko¨se composite pluton. Gondwana Res. 19, 926–944.

Dong, F.L., Mo, X.X., Yu, X.H., Hou, Z.Q., Wang, Y., 2007. Trace element geochemical and Nd–Sr–Pb isotope characteristics of the Zhuopan alkaline complex in Yongping, Yunnan Province and its geological significance. Acta Petrol. Sin. 23, 986–994 (in Chinese with English abstract).

Dostal, J., Chatterjee, A.K., 2000. Contrasting behaviour of Nb/Ta and Zr/Hf ratios in a peraluminous granitic pluton (Nova Scotia, Canada). Chem. Geol. 163, 207–218.

Elliott, T., Plank, T., Zindler, A., White, W., Bourdon, B., 1997. Element transport from slab to volcanic front at the Mariana arc. J. Geophys. Res. 102, 14991–15019.

Foley, S.F., Barth, M.G., Jenner, G.A., 2000. Rutile/melt partition coefficients for trace elements and an assessment of the influence of rutile on the trace element characteristics of subduction zone magmas. Geochim. Cosmochim. Acta 64, 933–938.

Gao, Y.F., Yang, Z.S., Santosh, M., Hou, Z.Q., Wei, R.H., Tian, S.H., 2010. Adakitic rocks from slab melt-modified mantle sources in the continental collision zone of southern Tibet. Lithos 119, 651–663.

Gill, J.B., 1981. Orogenic Andesite and Plate Tectonics. Springer-Verlag, Berlin, pp. 1–390.

Green, T.H., 1995. Significance of Nb/Ta as an indicator of geochemical processes in the crust–mantle system. Chem. Geol. 120, 347–359.

Gu, X.X., Tang, J.X., Wang, C.S., Chen, J.P., He, B.B., 2003. Himalayan magmatism and porphyry copper–molybdenum mineralization in the Yulong ore belt, East Tibet. Mineral. Petrol. 78, 1–20.

Guan, T., Huang, Z.L., Xu, C., Zhang, Z.L., Yan, Z.F., Chen, M., 2006. Ar-40-(39) Ar dating and geochemical characteristics of lamprophyres in the Baimazhai nickel deposit, Yunnan province. Acta Petrologica Sinica 22 (4), 873–883 (in Chinese with English abstract).

Hattori, K.H., Keith, J.D., 2001. Contribution of mafic melt to porphyry copper mineralization: evidence from Mount Pinatubo, Philippines, and Bingham Canyon, Utah, USA. Miner. Depos. 36, 799–806.

Hawkesworth, C., Turner, S., Peate, D., McDermott, F., VanCalsteren, P., 1997. Elemental U and Th variations in island arc rocks: implications for U-series isotopes. Chem. Geol. 139, 207–221.

Heinrich, C.A., Halter, W., Landtwing, M.R., Pettke, T., 2005. The formation of economic porphyry copper (–gold) deposits: constraints from microanalysis of fluid and melt inclusions. Miner. Depos. Earth Evol. 248, 247–263.

Hofmann, A.W., Jochum, K.P., 1996. Source characteristics derived from very incompatible trace elements in Mauna Loa and Mauna Kea basalts, Hawaii Scientific Drilling Project. J. Geophys. Res. Solid Earth 101, 11831–11839.

Horng, W.S., Hess, P.C., 2000. Partition coefficients of Nb and Ta between rutile and anhydrous haplogranite melts. Contrib. Mineral. Petrol. 138, 176–185.

Hou, Z.Q., Mo, X.X., Gao, Y.F., Qu, X.M., Meng, X.J., 2003a. Adakite, a possible host rock for porphyry copper deposits: case studies of porphyry copper belts in Tibetan Plateau and in northern Chile. Mineral Deposits 22, 1–12 (in Chinese with English abstract).

Hou, Z.Q., Ma, H.W., Zaw, K., Zhang, Y.Q., Wang, M.J., Wang, Z., Pan, G.T., Tang, R.L., 2003b. The Himalayan Yulong porphyry copper belt: product of large-scale strike-slip faulting in eastern Tibet. Econ. Geol. 98, 125–145.

Hou, Z.Q., Gao, Y.F., Qu, X.M., Rui, Z.Y., Mo, X.X., 2004. Origin of adakitic intrusives generated during mid-Miocene east–west extension in southern Tibet. Earth Planet. Sci. Lett. 220, 139–155.

Hou, Z.Q., Zeng, P.S., Gao, Y.F., Du, A.D., Fu, D.M., 2006. Himalayan Cu–Mo–Au mineralization in the eastern Indo–Asian collision zone: constraints from Re–Os dating of molybdenite. Miner. Depos. 41, 33–45.

Hou, Z.Q., Pan, X.F., Yang, Z.M., Qu, X.M., 2007. Porphyry Cu–(Mo–Au) deposits not related to oceanic-slab subduction: examples from Chinese porphyry deposits in continental setting. Geosci. 21, 332–351 (in Chinese with English abstract).

Hou, Z.Q., Zhang, H.R., Pan, X.F., Yang, Z.M., 2011. Porphyry Cu (–Mo–Au) deposits related to melting of thickened mafic lower crust: examples from the eastern Tethyan metallogenic domain. Ore Geol. Rev. 39, 21–45.

Hou, Z.Q., Zheng, Y.C., Yang, Z.M., Rui, Z.Y., Zhao, Z.D., Jiang, S.H., Qu, X.M., Sun, Q.Z., 2013. Contribution of mantle components within juvenile lower-crust to collisional zone porphyry Cu systems in Tibet. Miner. Depos. 48, 173–192.

Hu, R.Z., Burnard, P.G., Turner, G., Bi, X.W., 1998. Helium and argon systematics in fluid inclusions of Machangqing copper deposit in west Yunnan province, China. Chem. Geol. 146, 55–63.

Hu, R.Z., Burnard, P.G., Bi, X.W., Zhou, M.F., Pen, J.T., Su, W.C., Wu, K.X., 2004. Helium and argon isotope geochemistry of alkaline intrusion-associated gold and copper deposits along the Red River–Jinshajiang fault belt, SW China. Chem. Geol. 203, 305–317.
Huang, B., Liang, H.Y., Mo, J.H., Xie, Y.W., 2009. Zircon LA–ICP–MS U–Pb age of the Jinping–Tongchang porphyry associated with Cu–Mo mineralization and its geological implication. Geotecton. Metallog. 33, 598–602 (in Chinese with English abstract).
Huebner, J.S., Sato, M., 1970. Oxygen fugacity-temperature relationships of manganese oxide and nickel oxide buffers. Am. Mineral. 55, 934–952.
Imai, A., 2002. Metallogenesis of porphyry Cu deposits of the western Luzon arc, Philippines: K–Ar ages, SO_3 contents of microphenocrystic apatite and significance of intrusive rocks. Resour. Geol. 52, 147–161.
Imai, A., 2004. Variation of Cl and SO_3 contents of microphenocrystic apatite in intermediate to silicic igneous rocks of Cenozoic Japanese island arcs: implications for porphyry Cu metallogenesis in the Western Pacific Island arcs. Resour. Geol. 54, 357–372.
Imai, A., Listanco, E.L., Fujii, T., 1993. Petrologic and sulfur isotopic significance of highly oxidized and sulfur-rich magma of Mount Pinatubo, Philippines. Geology 21, 699–702.
Ionov, D.A., Hofmann, A.W., 1995. Nb–Ta-rich mantle amphiboles and micas-implications for subduction-related metasomatic trace-element fractionations. Earth Planet. Sci. Lett. 131, 341–356.
Jahn, B.M., Wu, F.Y., Lo, C.H., Tsai, C.H., 1999. Crust–mantle interaction induced by deep subduction of the continental crust: Geochemical and Sr–Nd isotopic evidence from post-collisional mafic–ultramafic intrusions of the northern Dabie complex, central China. Chem. Geol. 157, 119–146.
Jiang, Y.H., Jiang, S.Y., Ling, H.F., Dai, B.Z., 2006. Low-degree melting of a metasomatized lithospheric mantle for the origin of Cenozoic Yulong monzogranite-porphyry, east Tibet: geochemical and Sr–Nd–Pb–Hf isotopic constraints. Earth Planet. Sci. Lett. 241, 617–633.
Johnson, M.C., Plank, T., 1999. Dehydration and Melting Experiments Constrain the Fate of Subducted Sediments. http://dx.doi.org/10.1029/1999GC000014 (G3 1:1007-1026).
Kilinc, A., Carmichael, I.S.E., Rivers, M.L., Sack, R.O., 1983. The ferric-ferrous ratio of natural silicate liquids equilibrated in air. Contrib. Mineral. Petrol. 83, 136–140.
Klemme, S., Prowatke, S., Hametner, K., Gunther, D., 2005. Partitioning of trace elements between rutile and silicate melts: implications for subduction zones. Geochim. Cosmochim. Acta 69, 2361–2371.
La Flèche, M.R., Camire, G., Jenner, G.A., 1998. Geochemistry of post-Acadian, carboniferous continental intraplate basalts from the Maritimes Basin, Magdalen Islands, Quebec, Canada. Chem. Geol. 148 (115–136).
Lee, J.K.W., Williams, I.S., Ellis, D.J., 1997. Pb, U and Th diffusion in natural zircon. Nature 390, 159–162.
Leng, C.B., Zhang, X.C., Zhong, H., Hu, R.Z., Zhou, W.D., Li, C., 2013. Re–Os molybdenite ages and zircon Hf isotopes of the Gangjiang porphyry Cu–Mo deposit in the Tibetan Orogen. Miner. Depos. 48, 585–602.
Li, J.X., Qin, K.Z., Li, G.M., Cao, M.J., Xiao, B., Chen, L., Zhao, J.X., Evans, N.J., McInnes, B.I.A., 2012. Petrogenesis and thermal history of the Yulong porphyry copper deposit, Eastern Tibet: insights from U–Pb and U–Th/He dating, and zircon Hf isotope and trace element analysis. Miner. Petrol. 105, 201–221.
Li, H.G., 2009. Space-Time framework of structure-magma-minerlaization of alkali-rich porphyry Mo-Cu-Au polymetallic deposit in Boxingchang, Yunan Province. Ph.D. thesis, China University of Geosciences. Beijing, pp 76 (in Chinese with English abstract).
Liang, H.Y., Campbell, I.H., Allen, C., Sun, W.D., Liu, C.Q., Yu, H.X., Xie, Y.W., Zhang, Y.Q., 2006a. Zircon Ce^{4+}/Ce^{3+} ratios and ages for Yulong ore-bearing porphyries in eastern Tibet. Miner. Depos. 41, 152–159.
Liang, H.Y., Yu, H.X., Mo, C.H., Zhang, Y.Q., Xie, Y.W., 2006b. Zircon LA–ICP–MS U–Pb age, Ce^{4+}/Ce^{3+} ratios and the geochemical features of the Machangqing complex associated with copper deposits. Chin. J. Geochem. 25, 223–229.
Liang, J.L., Ding, X., Sun, X.M., Zhang, Z.M., Zhang, H., Sun, W.D., 2009. Nb/Ta fractionation observed in eclogites from the Chinese Continental Scientific Drilling Project. Chem. Geol. 268, 27–40.
Liu, Y.S., Hu, Z.C., Gao, S., Günther, D., Xu, J., Gao, C.G., Chen, H.H., 2008. In situ analysis of major and trace elements of anhydrous minerals by LA–ICP–MS without applying an internal standard. Chem. Geol. 257, 34–43.
Liu, Y.S., Gao, S., Hu, Z.C., Gao, C.G., Zong, K.Q., Wang, D.B., 2010a. Continental and oceanic crust recycling-induced melt–peridotite interactions in the trans-north China orogen: U–Pb dating, Hf isotopes and trace elements in zircons from mantle xenoliths. J. Petrol. 51, 537–571.
Liu, Y.S., Hu, Z.C., Zong, K.Q., Gao, C.G., Gao, S., Xu, J.A., Chen, H.H., 2010b. Reappraisement and refinement of zircon U–Pb isotope and trace element analyses by LA–ICP–MS. Chin. Sci. Bull. 55, 1535–1546.
Liu, X., Fan, H.R., Santosh, M., Hu, F.F., Yang, K.F., Li, Q.L., Yang, Y.H., Liu, Y.S., 2012. Remelting of Neoproterozoic relict volcanic arcs in the Middle Jurassic: implication for the formation of the Dexing porphyry copper deposit, Southeastern China. Lithos http://dx.doi.org/10.1016/j.lithos.2012.05.018.
Lu, Y.J., Kerrich, R., Kemp, A.I.S., McCuaig, T.C., Hou, Z.Q., Hart, C.J.R., Li, Z.X., Cawood, P.A., Bagas, L., Yang, Z.M., Cliff, J., Belousova, E.A., Jourdan, F., Evans, N.J., 2013. Intracontinental Eocene-Oligocene porphyry Cu mineral systems of Yunnan, Western Yangtze Craton, China: compositional characteristics, sources, and implications for continental collision metallogeny. Econ. Geol. 108, 1541–1576.
McInnes, B.I.A., Cameron, E.M., 1994. Carbonated, alkaline hybridizing melts from a subarc environment: mantle wedge samples from the Tabar-Lihir-Tanga-Feni arc, Papua New Guinea. Earth Planet. Sci. Lett. 122, 25–141.
Metrich, N., Clocchiatti, R., 1996. Sulfur abundance and its speciation in oxidized alkaline melts. Geochim. Cosmochim. Acta 60, 4151–4160.
Mitchell, A.H., 1973. Metallogenic belts and angle of dip of Benioff zones. Nature 245, 49–52.
Mo, X.X., Pan, G.T., 2006. From the Tethys to the formation of the Qinghai–Tibet Plateau: constrained by tectono-magmatic events. Earth Sci. Front. 13, 43–51 (in Chinese with English abstract).
Muller, D., 2002. Gold–copper mineralization in alkaline rocks—preface. Miner. Depos. 37, 1–3.
Muller, D., Groves, D.I., 1993. Direct and indirect association between potassic igneous rocks, shoshonites and gold–copper deposits. Ore Geol. Rev. 8, 383–406.
Mungall, J.E., 2002. Roasting the mantle: slab melting and the genesis of major Au and Au-rich Cu deposits. Geology 30, 915–918.
No. 15 Geological Survey Team (GST) of Yunan Geological Bureau, 1973. A Reserve Report of the Tongchang and Chang'anchong Copper–Molybdenite Deposits. pp. 1–8.
Oyarzun, R., Marquez, A., Lillo, J., Lopez, I., Rivera, S., 2001. Giant versus small porphyry copper deposits of Cenozoic age in northern Chile: adakitic versus normal calc-alkaline magmatism. Miner. Depos. 36, 794–798.
Oyarzun, R., Lillo, J., Oyarzun, J., 2008. No water, no cyanobacteria–No calc-alkaline magmas: progressive oxidation of the early oceans may have contributed to modernize island-arc magmatism. Int. Geol. Rev. 50, 885–894.
Pan, G.T., Chen, Z.L., Li, X.Z., Xu, Q., Jiang, X.S., 1996. Models for the evolution of the polyarc-basin systems in eastern Tethys. Lithofacies Palaeogeogr. 16, 52–65 (in Chinese with English abstract).
Pan, G.T., Xu, Q., Hou, Z.Q., Wang, L.H., Du, D.X., Mo, X.X., Li, D.M., Wang, M.J., Li, X.Z., Jiang, X.S., Hu, Y.Z., 2003. Archipelagic Orogenesis, Metallogenic Systems and Assessment of the Mineral Resources Along the Nujiang–Lanchangjiang–Jinshajiang Area in Southwestern China. Geologic Publishing House, Beijing, pp. 30–40 (in Chinese with English abstract).
Peacock, S.M., 1993. Large-scale hydration of the lithosphere above subducting slabs. Chem. Geol. 108, 49–59.
Pearce, J.A., Peate, D.W., 1995. Tectonic implications of the composition of volcanic arc magmas. Ann. Rev. Earth Planet. Sci. Lett. 23, 251–286.
Pfänder, J.A., Munker, C., Stracke, A., Mezger, K., 2007. Nb/Ta and Zr/Hf in ocean island basalts—implications for crust–mantle differentiation and the fate of Niobium. Earth Planet. Sci. Lett. 254, 158–172.
Plank, T., Langmuir, C.H., 1998. The chemical composition of subducting sediment and its consequences for the crust and mantle. Chem. Geol. 145, 325–394.
Qi, L., Hu, J., Grégoire, D.C., 2000. Determination of trace elements in granites by inductively coupled plasma mass spectrometry. Talanta 51, 507–513.
Richards, J.P., 1990. Petrology and geochemistry of alkaline intrusives at the Porgera gold deposit, Papua New Guinea. J. Geochem. Explor. 35, 141–199.
Richards, J.P., 2003. Tectono-magmatic precursors for porphyry Cu–(Mo–Au) deposit formation. Econ. Geol. 98, 515–1533.
Richards, J.P., 2009. Postsubduction porphyry Cu–Au and epithermal Au deposits: products of remelting of subduction-modified lithosphere. Geology 37, 247–250.
Richards, J.P., 2011. Magmatic to hydrothermal metal fluxes in convergent and collided margins. Ore Geol. Rev. 40, 1–26.
Rudnick, R.L., Fountain, D.M., 1995. "Nature and composition of the continental crust: A lower crustal perspective. Rev. Geophys. 33 (3), 267–309.
Sack, R.O., Carmichael, I.S.E., Rivers, M., Ghiorso, M.S., 1980. Ferric-ferrous equilibria in natural silicate liquids at 1 bar. Contrib. Mineral. Petrol. 75, 369–376.
Schmidt, M.W., Dardon, A., Chazot, G., Vannucci, R., 2004. The dependence of Nb and Ta rutile-melt partitioning on melt composition and Nb/Ta fractionation during subduction processes. Earth Planet. Sci. Lett. 226, 415–432.
Sillitoe, R.H., 1972. A plate tectonic model for the origin of porphyry copper deposits. Econ. Geol. 67, 184–197.
Sillitoe, R.H., 1997. Characteristics and controls of the largest porphyry copper–gold and epithermal gold deposits in the circum-Pacific region. Aust. J. Earth Sci. 44, 373–388.
Sillitoe, R.H., 2002. Some metallogenic features of gold and copper deposits related to alkaline rocks and consequences for exploration. Miner. Depos. 37, 4–13.
Sillitoe, R.H., 2010. Porphyry copper systems. Econ. Geol. 105, 3–41.
Spooner, E.T.C., 1993. Magmatic sulphide/volatile interaction as a mechanism for producing chalcophile element enriched, Archean Au-quartz, epithermal Au–Ag and Au skarn hydrothermal ore fluids. Ore Geol. Rev. 7, 359–379.
Stern, C.R., Funk, J.A., Skewes, M.A., Arevalo, A., 2007. Magmatic anhydrite in plutonic rocks at the El Teniente Cu–Mo deposit Chile, and the role of sulfur- and copper-rich magmas in its formation. Econ. Geol. 102, 1335–1344.
Streck, M.J., Dilles, J.H., 1998. Sulfur evolution of oxidized arc magmas as recorded in apatite from a porphyry copper batholith. Geology 26, 523–526.
Sun, S.S., Mcdoonough, W.F., 1989. Chemical and isotopic systematics of oceanic basalts: implication for mantle composition and processes. Geol. Soc. Spec. Pub. 42, 313–345.
Sun, W.D., Arculus, R.J., Kamenetsky, V.S., Binns, R.A., 2004. Release of gold-bearing fluids in convergent margin magmas prompted by magnetite crystallization. Nature 431, 975–978.
Sun, W.D., Liang, H.Y., Ling, M.X., Zhan, M.Z., Ding, X., Zhang, H., Yang, X.Y., Li, Y.L., Ireland, T.R., Wei, Q.R., Fan, W.M., 2013. The link between reduced porphyry copper deposits and oxidized magmas. Geochim. Cosmochim. Acta 103, 263–275.
Tatsumi, Y., 1989. Migration of fluid phases and genesis of basalt magmas in subduction zones. J. Geophys. Res. Solid Earth Planets 94, 4697–4707.
Tatsumi, Y., Hamilton, D.L., Nesbitt, R.W., 1986. Chemical characteristics of fluid phase released from a subducted lithosphere and the origin of arc magmas: evidence from high pressure experiments and natural rocks. J. Volcanol. Geotherm. Res. 29, 293–309.
Ulrich, T., Heinrich, C.A., 2001. Geology and alteration geochemistry of the porphyry Cu–Au deposit at Bajo de la Alumbrera, Argentina. Econ. Geol. 96, 1719–1742.
Ulrich, T., Guether, D., Heinrich, C.A., 1999. Gold concentrations of magmatic brines and the metal budget of porphyry copper deposit. Nature 399, 676–679.
Wallace, P.J., Carmichael, I.S.E., 1994. S-speciation in submarine basaltic glasses as determined by measurements of SK-alpha X-ray wavelength shifts. Am. Mineral. 79, 161–167.
Wang, J.H., Yin, A., Harrison, T.M., Grove, M., Zhang, Y.Q., Xie, G.H., 2001. A tectonic model for Cenozoic igneous activities in the eastern Indo–Asian collision zone. Earth Planet. Sci. Lett. 88, 123–133.

Wang, D.H., Qu, W.J., Li, Z.W., Ying, H.L., Chen, Y.C., 2004. The metallogenic concentrating epoch of the Porphyry Copper (molybdenum) deposits in Jinshajiang–Red River metallogenic belt: Re–Os isotope dating. Sci. China 34, 345–349 (in Chinese).
Wang, L.L., Mo, X.X., Li, B., Dong, G.C., Zhao, Z.D., 2006. Geochronology and geochemistry of the ore-bearing porphyry in Qulong Cu(Mo) ore deposit, Tibet. Acta Petrol. Sin. 22, 1001–1008 (in Chinese with English abstract).
Wones, D.R., 1989. Significance of the assemblage Titanite + Magnetite + Quartz in granitic-rocks. Am. Mineral. 74, 744–749.
Wones, D.R., Eugster, H.P., 1965. Stability of biotite: experiment, theory, and application. Am. Mineral. 50, 1228–1272.
Wybon, D., 1994. Sulfur undersaturated magmatism: a key factor for generating magma-related copper–gold deposits. AGSO. Res. Newsl. 21, 7–8.
Wyllie, P.J., 1978. Water and magma generation at subduction zones. Bull. Volcanol. 41, 360–377.
Xia, B., Lin, Q.C., Zhang, Y.Q., 2005. Zircon SHRIMP dating of diopside granite in Ailaoshan–Jinshajiang rock belt and its geological implications—example for Yuzhaokuai, Matouwan and Shlicun diopside granites. Geotecton. Metallog. 29, 35–43 (in Chinese with English abstract).
Xie, Y.W., Zhang, Y.Q., 1995. Petrochemistry of the Cenozoic magmatic rocks in the eastern Erhai, Yunan Province. Acta Petrol. Sin. 11, 423–433 (in Chinese with English abstract).
Xie, Y.W., Zhang, Y.Q., Zhong, S.L., Li, X.H., 1999. Trace element characteristics of the Cenozoic high-k alkaline magmatic rock series in the eastern Erhai, Yunnan Province. Acta Petrol. Sin. 15, 75–82 (in Chinese with English abstract).
Xiong, X.L., Adam, J., Green, T.H., 2005. Rutile stability and rutile/melt HFSE partitioning during partial melting of hydrous basalt: implications for TTG genesis. Chem. Geol. 218, 339–359.
Xu, L.L., 2011. The Diagenetic and Metallogenic Geochronology and Magmatic fO2 Characteristics of Jinshajiang–Red River Porphyry Cu(Mo–Au) Metallogenic Systems. (Ph.D. thesis), Institute of Geochemistry, Chinese Academy of Sciences, Guiyang (in Chinese with English abstract).
Xu, W.C., Zhang, H.F., Guo, L., Yuan, H.L., 2010. Miocene high Sr/Y magmatism, south Tibet: product of partial melting of subducted Indian continental crust and its tectonic implication. Lithos 114, 293–306.
Xu, L.L., Bi, X.W., Su, W.C., Qi, Y.Q., Li, L., Chen, Y.W., Dong, S.H., Tang, Y.Y., 2011. Geochemical characteristics and petrogenesis of the quartz syenite porphyry from Tongchang porphyry Cu(Mo–Au) deposit in Jinping County, Yunan Province. Acta Petrol. Sin. 27, 3109–3122 (in Chinese with English abstract).
Xu, L.L., Bi, X.W., Hu, R.Z., Zhang, X.C., Su, W.C., Qu, W.J., Hu, Z.C., Tang, Y.Y., 2012. Relationships between porphyry Cu–Mo mineralization in the Jinshajiang–Red River metallogenic belt and tectonic activity: constraints from zircon U–Pb and molybdenite Re–Os geochronology. Ore Geol. Rev. 48, 460–473.
Xu, L.L., Bi, X.W., Hu, R.Z., Tang, Y.Y., Jiang, G.H., Qi, Y.Q., 2014a. Origin of the ore-forming fluids of the Tongchang porphyry Cu–Mo deposit in the Jinshajiang–Red River alkaline igneous belt, SW China: constraints from He, Ar and S isotopes. J. Asian Earth Sci. 79, 884–894.
Xu, L.L., Bi, X.W., Hu, R.Z., Tang, Y.Y., Wang, X.S., Xu, Y., 2014b. LA–ICP–MS mineral chemistry of titanite and the geological implications for exploration of porphyry Cu deposits in the Jinshajiang–Red River alkaline igneous belt, SW China. Miner. Petrol. http://dx.doi.org/10.1007/s00710-014-0359-x.
Xue, B.G., 2008. On the division of Au metallogenetic zone and metallogenetic rule in Yunnan. Yunan Geol. 27, 261–277 (in Chinese with English abstract).
Yin, A., Harrison, T.M., 2000. Geologic evolution of the Himalayan–Tibetan orogen. Annu. Rev. Earth Planet. Sci. 28, 211–280.
Ying, J.F., Zhang, H.F., Sun, M., Tang, Y.J., Zhou, X.H., Liu, X.M., 2007. Petrology and geochemistry of Zijinshan alkaline intrusive complex in Shanxi Province, western North China Craton: implication for magma mixing of different sources in an extensional regime. Lithos 98, 45–66.
Zhang, Y.Q., Xie, Y.W., 1997. Nd, Sr isotopic characteristics and chronology of Ailaoshan–Jinshajiang alkali-rich intrusions. Sci. China (Ser. D) 27, 289–293 (in Chinese).
Zhang, H., Ling, M.X., Liu, Y.L., Tu, X.L., Wang, F.Y., Li, C.Y., Liang, H.Y., Yang, X.Y., Arndt, N.T., Sun, W.D., 2013. High oxygen fugacity and slab melting linked to Cu mineralization: evidence from dexing porphyry copper deposits, Southeastern China. J. Geol. http://dx.doi.org/10.1086/669975.
Zhao, X., Mo, X.X., Yu, X.H., Lu, B.X., Zhang, J., 2003. Mineralogical characteristics and petrogenesis of deep-derived xenoliths in Cenozoic syenite porphyry in Liuhe, western Yunnan Province. Earth Sci. Front. 10, 93–104 (in Chinese with English abstract).
Zheng, Y.Y., Gao, S.B., Cheng, L.J., Li, G.L., Feng, N.P., Fan, Z.H., Zhang, H.P., Guo, J.C., Zhang, G.Y., 2004. Finding and significances of Chongjiang porphyry copper (molybdenum, aurum) deposit, Tibet. Earth Sci. J. China Univ. Geosci. 29, 333–339 (in Chinese with English abstract).